

International Journal of Engineering (IJE)

ISSN : 1985-2312



VOLUME 2, ISSUE 1

PUBLICATION FREQUENCY: 6 ISSUES PER YEAR

Editor in Chief Dr. Kouroush Jenab

International Journal of Engineering (IJE)

Book: 2008 Volume 2, Issue 1

Publishing Date: 28-02-2008

Proceedings

ISSN (Online): 1985-2312

This work is subjected to copyright. All rights are reserved whether the whole or part of the material is concerned, specifically the rights of translation, reprinting, re-use of illustrations, recitation, broadcasting, reproduction on microfilms or in any other way, and storage in data banks. Duplication of this publication of parts thereof is permitted only under the provision of the copyright law 1965, in its current version, and permission of use must always be obtained from CSC Publishers. Violations are liable to prosecution under the copyright law.

IJE Journal is a part of CSC Publishers

<http://www.cscjournals.org>

©IJE Journal

Published in Malaysia

Typesetting: Camera-ready by author, data conversion by CSC Publishing Services – CSC Journals, Malaysia

CSC Publishers

Table of Contents

Volume 2, Issue 1, February 2008.

Pages

- 1 - 7 Implementing a Functional ISO 9001 Quality Management System
in Small and Medium-Sized Enterprises
Cory LP Searcy.
- 8 - 19 Study of the thermal behavior of a synchronous motor with
permanent magnets
Harmand Souad.
- 20 - 34 Finite Element Investigation of Hybrid and Conventional Knee
Implants
**Habiba Bougherara, Ziauddin Mahboob, Milan Miric,
Mohamad Youssef.**
- 35 - 41 Analytical Investigation of the Flow Hydrodynamics in Micro-
Channels at High Zeta Potentials
A. Elazhary, Hassan Soliman.
- 42 - 52 MFBLP Method Forecast for Regional Load Demand System
Zuhairi Baharudin, Nidal S. Kamel.

53 - 68

Generalized and Improved Relaxed Stabilization Conditions for
State Observer based Controller Systems in T-S Model with
Maximum Convergence Rate

Salem Abdallah, Zohra Kardous , Benhadj Braiek.

Intelligent GIS-Based Road Accident Analysis and Real-Time Monitoring Automated System using WiMAX/GPRS

Ahmad Rodzi Mahmud
Ehsan Zarrinbashar

Faculty of Engineering, University Putra Malaysia
43400 UPM Serdang, Malaysia

armcorp@gmail.com
ehsan_zarrinbashar@yahoo.com

Abstract

It has been a big concern for many people and government to reduce the amount of road accident specially in Malaysia since it could be a big threat to this country. Malaysian government has spent millions of money in order to reduce the number of accident occurrence through several modes of campaign. Unfortunately, from years to years the number keeps increasing. The lack of a comprehensive accident recording and analysis system in Malaysia can be effective in these kinds of problems. By making use of IRAS (Intelligent Road Accident System), the police would be control and manage whole accident events as a real-time monitoring system. This system exploits WiMAX and GPRS communications to connect to the server for transfer the specific data to the data center. This system can be used for a comprehensive intelligent GIS-based solution for accident analysis and management. The system is developed based on object and aspect oriented software design such as .NET technology.

Keyword: GIS, Accident, WiMAX, GPRS, LBS, Monitoring

1. Introduction

Road traffic accident is complicated to analyze as it crosses the boundaries of engineering, geography, and human behavior. Therefore, there is a need for a more systematic approach, which can automatically detect statistically significant spatial accident clusters and offering repeatable results. To implement traffic accident countermeasures effectively and efficiently, it is important to identify accident-prone locations and to analyze accident patterns so that the most appropriate measures can be taken for each specific location.

2. Research Motivation

The research undertaken intends to find a completed solution to covering all aspects in managing and monitoring accident data. The system is based on GIS and telecommunications infrastructures technologies. In this case, IRAS (Intelligent Road Accident System) is used to get the better results from accident data, which includes the most effective and useful queries, reports, charts and advanced graphical user interface. The work evaluates for performance of a GIS-based solution in order to integrate infrastructure communication systems such as WiMAX and GPRS to develop a multiplatform middle-ware for real-time monitoring, automated services. The development is based on aspect and object oriented software design. In addition, the other objective is to be established a dataware house for the real-time smart decision support system for automated services and analysis. Also, this system offers Location Based Services (LBS) for Clients' cell phone, PDAs, smart phones and laptops.

3. System Architecture

3.1. Enabling Telegeoinformatics

Telegeoinformatics is enabled through advanced in such fields as ge positioning, mobile computing, and wireless networking. There are different architectures possible for Telegeoinformatics, but one that is expected to be widely used is based on a distributed mobile computing environment where clients are location aware, that is capable of determining their location in real-time, and interconnected to intermediary servers via WiMAX/GPRS or even wired networks.

Telegeoinformatics can be based on different architectures to meet different requirements of applications, where clients and servers are connected via wireless networks. The middleware is used for performing many computations and activities and linking the different components of Telegeoinformatics. One of the key responsibilities of the middleware is ensuring interoperability among heterogeneous data, software, and functions. Figure 1 shows an ideal middleware for Telegeoinformatics.

3.2. Interoperability of Telegeoinformatics

In order to make Telegeoinformatics interoperable, the middleware must be based on special mechanism and protocols. Insomuch as geospatial data and geoprocessing are central to Telegeoinformatics, providing geospatial interoperability, eg., in Location-Based Services (LBSs) led by the Open GIS Consortium (OGC), should be one of the objectives of the middleware (OpenLS, 2001).

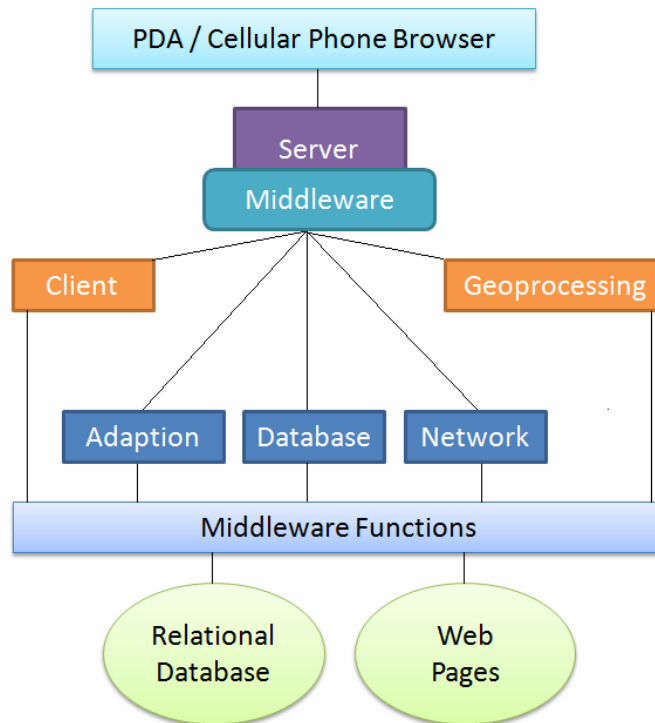


Figure 1: Telegeoinformatics Architecture

3.3. Strategies and Adaptation

One adaptation strategy in Telegeoinformatics is to adapt to the client machine the user would use to access the system. There are several client variations: PDA, Desktop PC, laptop, cell phone. Differences include storage capacity, processing power and user interface. Telegeoinformatics should have knowledge about these client's limitations with respect to the output interface and adjust its output information presentation to the capabilities available. Heineman (1999) has analyzed and evaluated various adaptation techniques for software components. On such technique is active interface. This

technique acts on port requests between software components, which is where method request are received. Another technique is Automatic Path Creation (APC), which is a data format, and routing technique that allows multi data format adaptation and adapts to current network conditions (Zao and Katz, 2002). Adaptation is not the modification of components by system designers; this is considered component evolution. Adaptation should be accomplished automatically by the system with little user intervention. In addition, adaptation should be considered a design capable of adapting to users with respect to the user's needs (Stephanidis, 2001).

3.4. Terminal-Centric Positioning

The Terminal-Centric methods rely on the positioning software installed in the mobile terminal. The method, which is used in this research, is Network Assisted GPS (A-GPS); this method can also be used in the network-centric mode, according to Andersson (2001). A-GPS uses an assisting network of GPS receivers that can provide information enabling a significant reduction of the time-to-first-fix (TTFF) from 20-45 s, to 1-8 s, so the receiver does not need to wait until the broadcast navigation message is read. It only needs to acquire the signal to compute its position almost instantly. For the timing information to be available through the network, the network and GPS would have to be synchronized to the same time reference. According to Andersson (2001) the assistance data is normally broadcast every hour, and thus it has a very little impact on the network's operability.

3.5. Network-Centric and Hybrid Positioning

Cell Global Identity with Timing Advance (CGI-TA) is one of the network-centric and hybrid positioning methods, which is used in this research. CGI uses the cell ID to locate the user within the cell, where the cell is defined as a coverage area of a base station (the tower nearest to the user). It is an inexpensive method, compatible with the existing devices, with the accuracy limited to the size of the cell, which may range from 10-500 m indoor micro cell to an outdoor macro cell reaching several kilometers (Andersson, 2002). CGI is often supplemented by the Timing Advance (TA) information that provides the time between the start of the radio frame and the data burst. This enables the adjustment of a mobile set's transmit time to correctly align the time, at which its signal arrives at the base (Snap Track, 2002).

4. Network-Based Service

The deployment of wireless-based LBSs relies on a common standards-based network infrastructure. The telecom market is currently experiencing a transition in the delivery of services from proprietary and network closed implementations to an open, IP-based service environment. The positioning service will be an important component in this open, IP-based service environment. The building of positioning information with LBSs, personalization, security, and messaging will be key for any operator when offering service packaging to the clients. The LBSs request/response flow is generally carried out within a wireless carrier network that includes mobile phone, the wireless network, the positioning server, gateway servers, geospatial server and the LBS application. The mobile phone provides a keypad for query and either a numeric or graphical interface for display. The positioning server, usually embedded in the wireless carrier's infrastructure, calculates the position of the device using one or more positioning approaches. The various wireless location measurement technologies fall into two broad categories: network-based and handset-based solutions (Campbell, 2001). Network-based solutions rely on base station radios to triangulate the position of a roaming mobile device, either with received radio signals or with transmitted synchronization pulses. The advantage of this approach is that it enables every user to access LBS without the need to upgrade the handset. Handset-based solution are systems that incorporate the measuring and processing of the location information within the handset. GPS is the principal technology and has been further enhanced by the development of A-GPS, which allows faster and more accurate service (Moeglein, 2001).

5. Multi Criteria Decision Making (MCDM)

The MCDM tool, which is embedded in server-side application, indicates AHP (Analytical Hierarchy Process) method, which can be used for decision making in GIS-based solution using input numeric values by the user. This tool is based on pairwise comparison method that developed by Tomas Saaty in 1970 in context of MADM (which is refer to attributes) method. It represents a theoretically founded approach to computing weights that are representing the relative importance of criteria. In this technique, weights are not assigning directly, but represent a “best fit” set of weights derived from the eigenvector of square reciprocal matrix. The objective of the AHP is to ensure that evaluation of weighting is consisted or not.

The AHP relies on three fundamental assumptions:

- i. Preferences for different alternatives depend on separate criteria, which can be reasoned about independently and given numerical scores.
- ii. The score for a given criteria can be calculated from sub-criteria. That is, the criteria can be arranged in a hierarchy and the score at each level of hierarchy can be calculated as a weighted sum of the lower level scores.
- iii. Suitable scores can be calculated from only pairwise comparisons.

AHP is a mathematical decision making technique that allows consideration of both qualitative and quantitative aspects of decisions. It reduces complex decisions to a series of one-on-one comparisons, and then synthesizes the results. Compared to other techniques like ranking and rating, the AHP uses the human ability to compare single properties of alternatives, it not only helps decision makers choose the best alternative, but also provides a clear rational for the choice.

6. Methodology

The develop system consist of the main module that operate as a real-time monitoring system. The system started with a field data collection which perform as client. All data which are related to accident, can be categorizes into spatial data and non-spatial data which are merged into one database. The merged data is transferred to the dataware house via internet by using WiMAX/GPRS. Dataware house will then be established with two different reference of data includes Road Networks (map data) and Datacenter (description data). The main system uses integrated data from the dataware house and analyzes on them to achieve various types of statistical reports, these reports can be customized and improved with different elements by interaction through the designed GUI.

The main system will be able to recycle the outcome of the primary analyses into the system and pass the statistical reports to MCDM unit (Multi Criteria Decision Making). Under the module, AHP (Analytical Hierarchy Process) technique is used for decisions making process. The results will then be used in the next module, which is SDM (Smart Decision Maker). In this module, reports can be compared together, make the best decision for diagnosis, and define the proposed solution related to current situation. SDM unit has potential to modeling suggested solution based on GIS interface. Figure 2 shows the process and relations between main system and the other parts to provide the proposed solution.

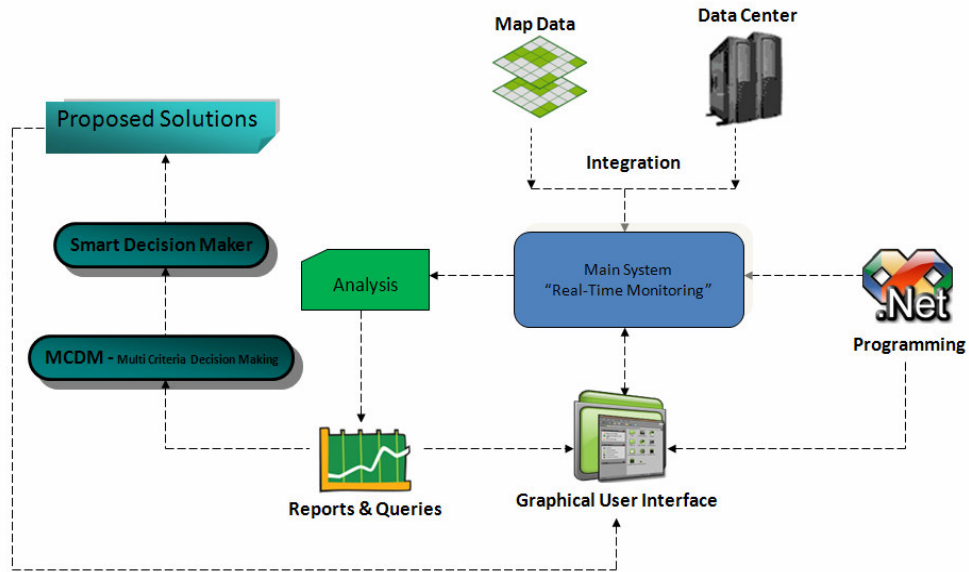


Figure 2: The relationship between main system and MCDM and SDM modules

There are two types of clients that should be defined to the system, Police and end users (citizens). After each accident, the clients (citizens) can provide necessary information to the main system by using their Mobile Phone (SMS) or using their PDA (WiMAX/GPRS). The main system automatically will search and announce the nearest police vehicle via internet around the accident location and suggest the best path to get to the accident location based on the traffics information, time and distance. In this case, police officers using PDA via internet directly to the main system will key all accident information in and then the system will automatically send data to the dataware house and update the database. Also at the same time, system will be able to inform other involved organizations and companies such as medical emergency services, insurance and car service companies. Figure 3 shows the relationship between main system and clients.

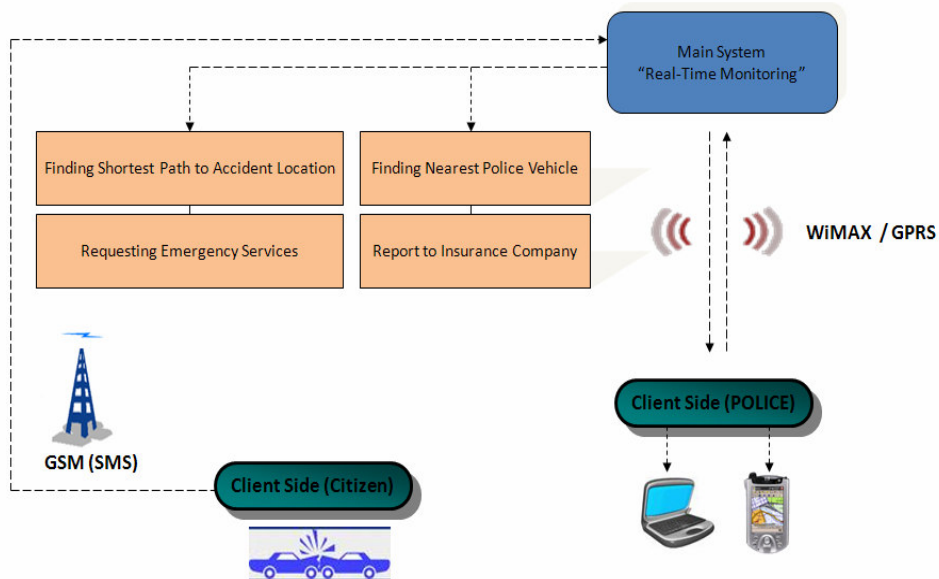


Figure 3: The relationship between main system and clients

7. Results and Discussion

The system being developed manage to support online communication through the GSM/GPRS/WiMAX services. User who wants to use this system must have a few equipments on his/her car which call On-Board Unit (OBU). These equipments consist of GPS and wireless communication devices. The main system also consists of Auto Alarming System (AAS) to inform the system for any accident events throughout the city. In this case, when an accident occurs, the location of the accident sends to the main system by client (citizen) using GPS devices installed on the vehicle, this task is done by calling OBU which, automatically or manually send the accident position to the server via internet using WiMAX or GPRS. From the signal received, the system will find the nearest police vehicle according to the accident coordinate system and sends the primary information to client (police officer) in their PDAs via internet. Then, accident data will be send to data center and store on the system and dataware house. This system can send online data to road accident database using PDA or Smartphone by police officers in real time access. In addition, Smart Decision Making (SDM), Multi Criteria Decision Making (MCDM) and Automatically Proposed solution system (APSS) units can be applied professionally and analytically for making the particular reports and queries in a proper manner.

8. Conclusion

The research outcome is a comprehensive system to cover accident management and analysis, smart automated service for accident locations, accident and service diagnosis, reducing the number of accidents, increasing the level of road safety and fast delivery services such as insurance companies and emergency services. For further works, the system should also include the ability to inform clients about the risk zones in all over the city using LBS services, based on the main system reports, queries and real time traffic monitoring. The system classifies and categorizes the road networks into four zones, so when a vehicle enter to each zone, the system will automatically send the risk message to alert the accident risk on that particular zone or location of the city. In addition, the system shall offer some services for clients such as air download client version (for PDAs or Smartphone) of application for using these LBS services. All LBS data, which will be shown on client phone, are generated by the main system with real time updates via internet, so the clients have real time information about the traffic conditions and accident risk zones around them.

9. References:

1. M.A. Abdel-Aty, A.E. Radwan. "Modelling traffic accident occurrence and involvement". Accident Analysis and Prevention, 32(5):633-642, 2000
2. C. Andersson. "Wireless Developer Network web page". Online. Available HTTP: <<http://wirelessdevnet.com/channels/lbs/features/mobileposition.html>> (Accessed on 25 Jan 2008).
3. B. Brumitt, B. Meyers, J. Krumm, A. Kern, and S. Shafer. "Easyliving: Technologies for intelligent environments". Second Int. Symp. On Handhelds and Ubiquitous Computing (HUC 200), pp. 12-29, Bristol, UK, 2000
4. A. Ceder, M. Livneh. "Relationships between road accidents and hourly traffic flow". Accident Analysis and Prevention, 14(1):19-34, 1986
5. E. Hauer. "On the estimation of the expected number of accidents". Accident Analysis and Prevention, 18(1):1-12, 1986
6. G.T. Heineman. "An Evaluation of Component adaptation Techniques, in 2nd ICSE workshop on Component-Based Software Engineering", Orlando, FL, 1999
7. Kh. Eldrandaly. "COM-based Spatial Decision Support System for Industrial Site Selection". Geographic Information and Decision Analysis, 7(2):72-92, 2003

8. U. Kubach. K. Rothermel. "Exploiting Location Information for Infostation-Based Hoarding, in Proceedings of the seventh ACM SIGMOBILE. Annual International Conference on Mobile Computing and Networking" Rome, Italy, pp. 15-27, 2001
9. P.C. Lai, W.Y. Chan. "GIS for Road Accident Analysis in Hong Kong" .Geographic Information Sciences, 10(1):58-67, 2004
10. M. Moeglein. "An Introduction to SnapTrack Server-Aided GPS Technology", SnapTrack, Campbell, CA. Online Available HTTP: <<http://www.snaptrack.com/AtWork/ion.pdf>> (Accessed on 23 Jan 2008), 2001
11. OpenLS (Open Location Services). Initiative. Online. Available HTTP: <<http://www.opengis.org/>> (Accessed on 20 Jan 2008), 2001
12. Snap Track, "Location Technologies for GSM, GPRS and WCDMA Networks". Online. Available HTTP: <http://snaptrack.com/advantage/location_tech_9_01.pdf > (Accessed on 25 Jan 2008), 2002
13. R.J. Stewart. "Applications of Classification and Regression Tree Methods in Roadway Safety Studies", 1996
14. C. Stephanidis. "Adaptive Techniques For Universal Access". User Modeling and User-Adapted Interaction, 11(1-2):159-197, 2001
15. Wireless World Forum (WWF), "Location-based services – long term optimism prevails".Online. Available HTTP: <[http:// www.w2forum.com/news/w2fnews10209.html](http://www.w2forum.com/news/w2fnews10209.html)> (accessed 10 Jan 2008), 2002
16. M. Zao, R, Katz. "Achieving service portability using self-adaptive data paths". IEEE Communications Magazine, 40(1):108-114, 2002

Effect Of Wire Mesh Orientation On Strength Of Beams Retrofitted Using Ferrocement Jackets

Prem Pal Bansal*, B.E. Civil, M.E, Civil (Structures)
Lecturer, Department of Civil engineering,
Thapar University, Patiala,
INDIA 147 004

* Corresponding Author

Dr. ManeeK Kumar, B.E. Civil, M.E, Civil (Structures),
Ph.D.
Professor & Head, Department of Civil engineering,
Thapar University, Patiala,
INDIA 147 004

prempalbansal@yahoo.co.in
prempal@gmail.com

maneeK@tiet.ac.in

Dr. S.K. Kaushik, B.Tech. Civil, M.E, Civil (Structures),
Ph.D.
Formerly Professor and Head, Department of Civil
Engineering,
Indian Institute of Technology, Roorkee
INDIA

Abstract

Various retrofitting techniques are used in field and out of all plate bonding technique is considered as the best. In this technique, the plates of different materials viz CFRP, GFRP, ferrocement etc are bonded to the surface of structural member to increase its strength. Ferrocement sheets are most commonly used as retrofitting material these days due to their easy availability, economy, durability, and their property of being cast to any shape without needing significant formwork. In the present work, effect of wire mesh orientation on the strength of stressed beams retrofitted with ferrocement jackets has been studied. The beams are stressed up to 75 percent of safe load and then retrofitted with ferrocement jackets with wire mesh at different orientations. The results show that the percent increase in load carrying capacity for beam retrofitted with ferrocement jackets with wire mesh at 0, 45, 60 degree angle with longitudinal axis of beam, varies from 45.87 to 52.29 percent. Also a considerable increase in energy absorption is observed for all orientations. However, orientation at 45 degree shows higher percentage increase in energy absorption followed by 60 and 0 degree respectively.

Keywords: ferrocement, retrofitting, jacket, wire mesh, orientation, beams.

1.0 INTRODUCTION

Reinforced concrete is one of the most abundantly used construction material, not only in the developed world, but also in the remotest parts of the developing world. The RCC structures constructed in the developed world are often found to exhibit distress and suffer damage, even before their service period is over due to several causes such as improper design, faulty construction, change of usage of the building, change in codal provisions, overloading, earthquakes, explosion, corrosion, wear and tear, flood, fire etc.

Such unserviceable structures require immediate attention, enquiry into the cause of distress and suitable remedial measures, so as to bring the structure into its functional use again.

In the last few decades several attempts have been made in India and abroad to study these problems and to increase the life of the structures by suitable retrofitting and strengthening techniques. Of the various retrofitting techniques available, plate bonding is one of the most effective and convenient methods of retrofitting. Among the plate bonding techniques FRP plates are quite popular now-a-days. But it is observed that the use of FRP is restricted to developed countries or urban areas of the developing countries due to higher initial cost and requirement of skilled labour for their application. Thus, there is a need to develop an alternative technique, which is economical and can be executed at site with the help of semi-skilled labour available at site. Ferrocement jacketing is found to be one such attractive technique due to its properties such as good tensile strength, lightweight, overall economy, water tightness, easy application and long life of the treatment.

Many experimental studies have been conducted in recent years to strengthen flexural members by using various materials. *Andrew and Sharma (1998)* in an experimental study compared the flexural performance of reinforced concrete beams repaired with conventional method and ferrocement. They concluded that beams repaired by ferrocement showed superior performance both at the service and ultimate load. The flexural strength and ductility of beams repaired with ferrocement was reported to be greater than the corresponding original beams and the beams repaired by the conventional method.

Beams rehabilitated with ferrocement jackets show better performance in terms of ultimate strength, first crack load, crack width, ductility and rigidity of the section. It was observed that the cracking and ultimate strength increases by 10 percent and 40 percent in case of rehabilitated beams, whereas these increases were 10-30 percent and 40-50 percent in case of composite sections. The jacketing increases the rigidity of the beams and lead to 37 percent and 29 percent reduction in deflection. The crack width of the composite beams and rehabilitated beams decreases on an average by 42 percent and 36 percent respectively [*Kaushik, S.K. and Dubey, A.K., 1994*].

The addition of thin layer of ferrocement to a concrete beam enhances its ductility and cracking strength. Composite beams reinforced with square mesh exhibit better overall performance compared to composite beams reinforced with hexagonal mesh. An increase in the number of layers improves the cracking stiffness of the composite beams in both cases. [*Nassif, H.H et al, 1998, Vidivelli, B. et al, 2001, Nasif, N.H. et al 2004*].

A ferrocement shell improves the flexural behaviour of RCC beams, although there is no increase in the moment carrying capacity of under reinforced beams. However, the moment carrying capacity increased by 9 per cent and 15 per cent for balanced and over reinforced sections respectively [*Seshu, D.R., 2000*].

The ultimate strength of the reinforced concrete beams, which failed due to overloading and were repaired using ferrocement laminate, is affected by the level of damage sustained prior to repairing. However, ultimate strength ductility ratio and energy absorption have been reported to improve after the repair in all cases. The steel ratio used in the repair layer has a great influence on the amount of gain in the resisting moment, ductility ratio and energy absorption. The higher the steel ratio the higher the gain in resisting moment and energy absorption; conversely, the ductility ratio was found to be decreased with increase in steel ratio [*Fahmy, Ezzat H. et al, 1997*].

Paramasivam, P. et al (1994) studied the flexural behavior of reinforced concrete T-beams strengthened with thin ferrocement laminate attached to the tension face using L-shaped mild steel round bars as shear connectors. From the experimental investigation it was concluded that after strengthening the performance of the beam improved substantially in terms of strength, flexural rigidity and first crack load, provided the connectors are adequately spaced

and the surface to receive the laminate roughened to ensure sufficient bond strength for composite action.

Thus, ferrocement is a viable alternative material for repair and strengthening of reinforced concrete structures. It has been accepted by the local building authority in Singapore for use in upgrading and rehabilitation of structures. The National Disaster Mitigation Agency (NDMA), Government of India, also accepted the use of ferrocement for this purpose.

The behaviour of ferrocement in flexure depends upon various parameters such as mortar, type of wire mesh, orientation of wire mesh etc.; hence the behaviour of ferrocement jackets. In the present paper the effect of wire mesh orientation on the strength, toughness and ductility of the retrofitted beams is presented.

2.0 EXPERIMENTAL PROGRAMME

To carry out the investigation, eight prototype beams of size 127mm x 227mm x 4100mm reinforced with two bars of 10 mm diameter in tension and two bars of 8mm diameter in compression were cast using the proportioned mix as shown in Fig.1. Out of these eight beams, two were used as control beams (Type- A) and tested to failure to find out the safe load carrying capacity corresponding to the allowable deflection as per *IS:456-2000* i.e. span /250. The other six beams were stressed to 75 percent of the safe load obtained from the testing of the control beams and were then retrofitted with 15 mm thick ferrocement jackets made with 1:2 cement sand mortar and w/c ratio 0.40 as shown in Fig. 2. The jacket was reinforced with single layer of 40mm x 40mm square welded wire mesh. The three wire mesh orientation viz. 0, 45, 60 degree were used in the ferrocement jackets.

The set of beams (two each) were divided into four categories depending upon the orientation of wire mesh in the jacket. Control beams were designated as type-A, whereas, beams retrofitted with welded wire mesh oriented at 0 degree were designated as type – B beams. Retrofitted beams having welded wire mesh oriented at 45 degrees and 60 degrees were designated as type – C and type-D, respectively. The same are shown in Plate 1

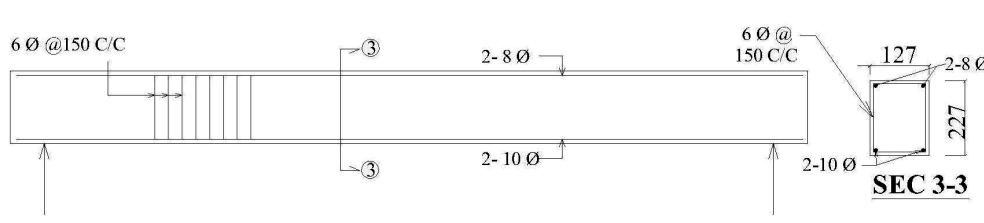


Fig. 1 Longitudinal and Cross-Section of Unretrofitted Under Reinforced Beams
(All Dimensions are in mm)

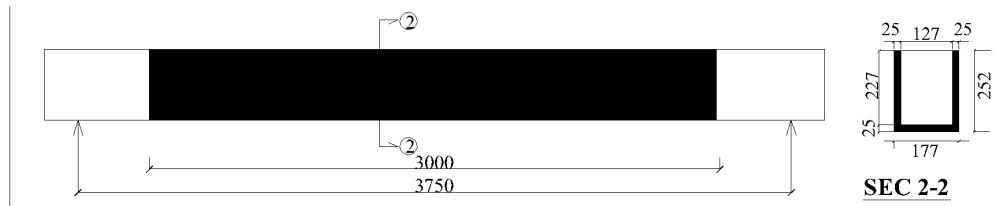
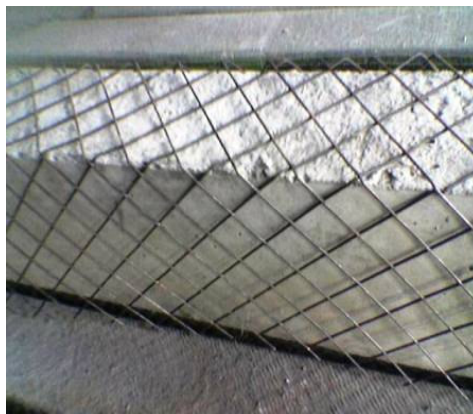


Figure 2: Longitudinal and Cross-Section of Retrofitted Beams



(a) 0° Orientation



(b) 45° Orientation



(c) 60° Orientation

Plate 2 Different Wire Mesh Orientations

2.1 Materials

The properties of various materials used in the experimental study are reported in Tables 1 to 4

Sr. No.	Characteristics	Test Values	Values as per IS:1489 (Part 1)
1	Standard consistency	34	-
2	Fineness of cement as retained on 90-micron sieve (%)	0.5	< 10
3	Setting time (mins) 1. Initial 2. Final	84 300	> 30 < 600
4	Specific gravity (Specific gravity bottle)	3.07	-
5	Compressive Strength (MPa) 1. 7days 2. 28 days	30.0 43.0	22.0 33.0
6	Soundness (mm) (by Le-Chatelier's method)	2.0	< 10 (Fresh Cement) < 5 (Old Cement)

Table 1: Physical Properties of Portland Pozzolana Cement

S. No.	Characteristics	Value
1.	Specific gravity (oven dry basis)	2.52
2.	Bulk density loose (kN/m ³)	14.8
3.	Fineness modulus	2.36
4.	Water Absorption (%)	2.67
5.	Grading Zone	Zone II

Table 2: Physical Properties of Fine Aggregates

Sr. No.	Characteristics	Value	
		CA-I	CA-II
1.	Type	Crushed	Crushed
2.	Maximum Nominal Size (mm)	12.5	4.75
3.	Specific gravity	2.68	2.70
4.	Total water absorption (%)	1.45	1.643
5	Fineness modulus	7.45	6.21

Table 3: Physical Properties of Coarse Aggregates

Sr. No.	Diameter of bars/ mesh wire (mm)	Yield-Strength (N/mm ²)	Ultimate Strength (N/mm ²)	Elongation (percent)
1.	12	452.00	584.00	23.00
2.	10	470.00	580.0	20.0
3.	8	445.00	555.0	23.0
4.	6	442.42	612.7	32.9
5.	2.4 mm	400	511.36	2.52

Table 4: Physical Properties of Steel Bars and Steel Mesh Wires

2.2 Testing Arrangement

All the eight simply supported beams were tested with an effective span of 3.75 m. Two concentrated loads were applied at 1m spacing for testing (see Fig -3). The beams were tested using hydraulically operated jacks connected to a data acquisition system through the load cells. With an increase in load the deflection in the beam was noted using three dial gauges placed at the quarter span points. The same is shown in Plate 2

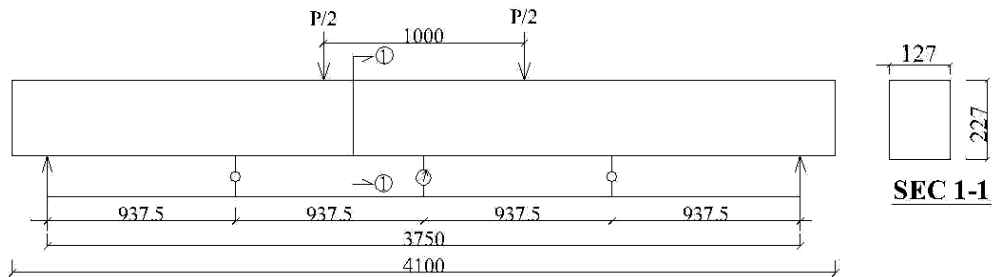


Fig. 3: Loading Arrangement for Testing of all Beam Specimens
(All Dimensions are in mm)



Plate 1: Test Setup

2.3 Process of retrofitting

Firstly the surface of beam is cleaned. After cleaning the surface, the cement slurry is applied as bonding agent to the surface of beam. After the application of bonding agent retrofitting of beam is done by applying 15mm thick cement mortar on the three faces as ferrocement jackets having wire mesh at different orientation. The beams are cured for 7days before testing. Then with same procedure as of control beam, testing of beam is done in order to calculate ultimate load and corresponding deflections.

3.0 RESULTS AND DISCUSSION

First, the two control beams were tested to failure. The load corresponding to an allowable central deflection of 15 mm (span/250) was obtained from load deflection curve as 12.67 kN. The remaining six beams were stressed to 75 percent of this average safe load i.e. 9.50 kN. Subsequently the retrofitting of beams using different orientations of wire mesh in the ferrocement jackets was carried out. These retrofitted beams were then loaded to failure and the data was recorded in the form of load and deflection. Table 5 presents this data for the control beams and beams retrofitted using specified wire mesh orientations. Fig 4 shows the load deflection behaviour at the mid span points of the control as well as beams retrofitted with different wire mesh orientations.

It is observed from the curves in Fig 4 that with an increase in load there is a considerable increase in deflection for all the beams. It was also noted that the spacing of cracks was 45mm in case of beams retrofitted with wire mesh at zero degree as compared to beams retrofitted with wire mesh at 45°, for which it was 85mm. The spacing increased to 108 mm for 60-degree orientation. This shows that the distribution of stress with wire mesh at zero degree is better. It is also observed that corresponding to the serviceability requirement of 15 mm deflection, the load increased from 12.67 kN for the control beam to 14.15 kN, 13.25 kN, 15.41 kN for type B, C and D retrofitted beams, respectively.

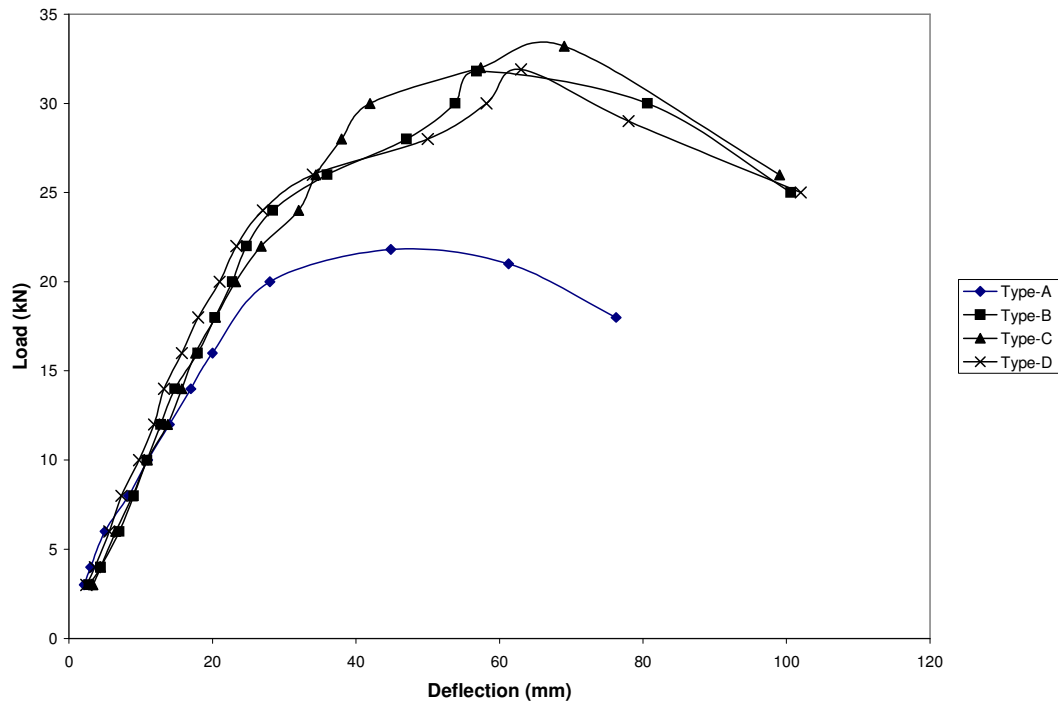


Figure 4: Load V/S. Deflection Curve At Mid Span For Control Beam And Beams Retrofitted With Wire Mesh At Different Orientations

It is also observed from the curves that the deflection at the centre at maximum load is maximum in the case of beams retrofitted with wire mesh at 45 degrees, which is 69.05mm as compared to those with wire mesh at zero degree, for which it is 56.82mm, and for 60 degree, for which it is 63.0 mm.

The load deflection curves were idealized as quadri-linear curves. Using the idealized curves the ductility ratio i.e. ratio of deflection at ultimate load to yield load, and energy absorption i.e. area under the curve up to ultimate load are calculated and presented in Table 6. It is observed that the ductility ratio increases by 4.47, 0.40 and 0.82 percent and energy absorption increases by 76.27, 73.98, and 70.42 percent for Type-B, Type-C and Type-D beams respectively as compared to the control beams (Type-A).

The results indicate that the beams retrofitted with wire mesh at 45 degree as reinforcement in the ferrocement jacket is best among all the three with regards to enhanced maximum load carrying capacity followed by 60 degree and zero degree respectively. However, the ductility ratio and energy absorption capacity is highest in case of beams retrofitted wire mesh at zero degree followed by forty-five degrees and sixty degrees. The increase in ductility ratio and energy absorption of beams retrofitted using ferrocement jacket having welded wire mesh at different orientations, as reinforcement are makes the retrofitted beams suitable for dynamic load applications.

S. No	Control Beam (Type –A ⁺⁺)			Beam with Wire Mesh at 0° (Type –B ⁺⁺)			Beam with Wire Mesh at 45° (Type –C ⁺⁺)			Beam with Wire Mesh at 60° (Type – D ⁺⁺)		
	Load (kN)	Deflection (mm) at		Load (kN)	Deflection (mm) at		Load (kN)	Deflection (mm) at		Load (kN)	Deflection (mm) at	
		L/2	L/4		L/2	L/4		L/2	L/4		L/2	L/4
1	3	2.1	1.20	3	2.8	1.8	3	3.35	2.12	3	2.43	1.82
2	4	3.0	1.82	4	4.4	3.0	4	4.42	3.0	4	3.58	2.4
3	6	5.0	3.02	6	7.0	4.89	6	6.50	4.5	6	5.61	3.16
4	8	8.3	5.00	8	9.0	6.48	8	8.87	6.0	8	7.30	4.20
5	10	10.98	7.00	10	10.87	7.76	10	10.9	7.74	10	9.76	4.87
6	12	14.0	9.22	12	12.8	9.2	12	13.75	9.26	12	11.85	6.0
7	14	17.0	11.2	14	14.76	10.15	14	15.75	11.45	14	13.24	7.76
8	16	20.0	13.50	16	17.95	13.42	16	17.63	13.98	16	15.73	9.84
9	20	28.0	19.00	18	20.34	15.36	18	20.42	16.76	18	18.00	11.95
10	21.8	44.85	33.4	20	22.76	16.9	20	23.2	17.5	20	21.00	13.72
11	21	61.28		22	24.76	18.5	22	26.8	21.0	22	23.33	15.0
12	18	76.28		24	28.4	20.22	24	32.0	25.0	24	27.00	17.5
13				26	36.0	24.0	26	34.4	28.0	26	34.00	24.0
14				28	47.05	32.04	28	38.0	31.45	28	50.00	36.34
15				30	53.82	-	30	41.95	35	30	58.20	41.52
16				31.8	56.82		32	57.37	40.2	31.9	63.0	45.51
17				30	80.62		33.2	69.05	42.82	29	78	
18				25	100.62		26	99.05		25	102	

Table 5: Load v/s. Deflection Data For Control Beam And Beams Retrofitted with Ferrocement Jacket having Welded Wire Mesh at Different Orientation

Sr. No	Beam type	P_{max} (kN)	M_{max} (kN-m)	Ductility Ratio*	Energy Absorption** (kN-m)	Increase in Energy Absorption (%)
1	Type-A**	21.8	14.99	2.46	1244.27	-
2	Type-B**	31.8	21.862	2.57	2193.22	76.27
3	Type-C**	33.2	22.825	2.46	2164.72	73.98
4	Type-D**	31.9	21.93	2.48	2120.45	70.42

Table 6: Test Results of Beams Retrofitted Using Ferrocement Jacket having Welded Wire Mesh at Different Orientation

* Ductility ratio of the beams is defined as ratio of deflection at ultimate load to the yield load calculated from idealized quadri-linear load deflection curve

** Area under the load deflection curve upto ultimate load

A detailed cost analysis to check the economic feasibility of different wire mesh orientations is presented in the succeeding section.

3.1 Cost Analysis

A comparative cost analysis for four types of beams is presented in Table 7.

It is noted that beams retrofitted with wire mesh oriented at zero degree are the most efficient of the three orientations as its cost to strength ratio is the lowest at 1.19 as compared to the other two orientations for which the value is 1.21 and 1.30 for wire mesh at 45 degrees and 60 degrees, respectively.

Thus, the beams retrofitted using ferrocement jackets having wire mesh orientation at zero degree are most efficient (lowest cost to strength ratio) as compared to other orientations.

4.0 CONCLUSIONS

Based upon the test results of the experimental study undertaken, the following conclusions may be drawn:

1. The beams retrofitted with wire mesh at different orientations do not de-bond when loaded to failure.
2. The failure of the composite is characterized by development of flexural cracks over the tension zone. The spacing of cracks is reduced for retrofitted beams indicating better distribution of stress.
3. Wire mesh orientated at 45 degree for retrofitting the stressed beams has the highest load carrying capacity as compared to control beam as well as the other beams retrofitted using different orientations.
4. After retrofitting, all the test specimens showed reduced crack widths, large deflection at the ultimate load, a significant increase in the ductility ratio, and considerable increase in the energy absorption as well, making the components better equipped to resist dynamic loads.
5. Beams retrofitted with wire mesh oriented at zero degree were the most efficient as their cost to strength ratio is lowest.

Material	Rate (Rs.)	Cost (Rs.) of Beam type			
		A ^{**}	B ^{**}	C ^{**}	D ^{**}
Concrete Ingredients					
Cement (kg)	215	215	215	215	215
Rebars (kg)					
10mm	30.10	148.724	148.724	148.724	148.724
8mm	30.75	97.14	97.14	97.14	97.14
6mm	33.75	111.52	111.52	111.52	111.52
Coarse Aggregates (cft)	14.0	50.89	50.89	50.89	50.89
Fine aggregates (cft)	17.0	29.56	29.56	29.56	29.56
Labour for control beams	Lump Sum	200	200	200	200
<i>Cost of Ingredients</i>		<i>852.834</i>	<i>852.834</i>	<i>852.834</i>	<i>852.834</i>
Retrofitting Material					
Welded Wire mesh	Lump Sum	-	330	420	480
Additional material like cement, Fine aggregates, screws etc.	Lump Sum	-	107	107	107
Labour	Lump Sum	-	192	192	192
<i>Cost of Retrofitting</i>		-	<i>629</i>	<i>719</i>	<i>779</i>
Total Cost		852.834	1481.834	1572.834	1631.834
Cost ratio		1.0	1.74	1.84	1.91
Strength Ratio		1.0	1.46	1.52	1.46
Cost/Strength Ratio		1.0	1.19	1.21	1.30

Table 7: Cost Analysis of Beams Retrofitted Using Ferrocement Jacket having Welded Wire Mesh at Different Orientations

- ^{**} Beam Type A = Control unretrofitted beam
 Beam Type B = Beam retrofitted with welded wire mesh oriented at zero degree
 Beam Type C = Beam retrofitted with welded wire mesh oriented at 45 degree
 Beam Type D = Beam retrofitted with welded wire mesh oriented at 60 degree

* The cost of the wire mesh at 45 degrees and 60 degrees orientation increases due to wastages at these angles

5.0 REFERENCES

1. Andrews, G., Sharma, A.K., "Repaired Reinforced Concrete Beams" ACI, Concrete International, pp. 47-50, 1998
2. Fahmy, Ezzat H., Shaheen, Youysry B.I. and Korany Yasser, S. "Repairing Reinforced Concrete Beams by ferrocement" Journal of Ferrocement: Vol. 27, No. 1, pp 19-32, January 1997.
3. IS: 456-2000, Indian Standard Plain and Reinforced Concrete-Code of Practice, Bureau of Indian Standards, New Delhi.
4. Kaushik, S.K. and Dubey, A.K. "Performance Evaluation of RC Ferrocement Composite Beams" Proceedings of Fifth International Symposium, UMIST, pp 240- 256, 1994

5. Nassif, H.H., Chirravuri, G. and Sanders, M.C. " Flexural Behavior of Ferrocement / Concrete Composite Beams" Ferrocement 6: Lambot Symposium, Proceedings of the Sixth International Symposium on Ferrocement, Universty of Michigan, Michigan USA, pp251 – 258, June 1998.
6. Nassif, Hani H. and Najm, Husam, "Experimental and analytical Investigation of Ferrocement-Concrete Composite" Cement and Concrete Composite, Vol. 26, pp 787-796, 2004.
7. Paramasivam, P., Ong, K.C.G. and Lim, C.T.E., "Ferrocement Laminate for Strengthening of RC T-Beams" Cement and Concrete Composite, Vol. 16, pp 143-152, 1994.
8. Seshu, D.R. " Flexural Behavior of Ferrocement Confined Reinforced Concrete (FCRC) Simply Supported Beams" Journal of Ferrocement: Vol. 30, No. 3, pp 261-273, July 2000.
9. Vidivelli, B., Antiny Jeyasehar, C., and Srividya, P.R., " Repair and Rehabilitation of Reinforced Concrete Beams by Ferrocement" Seventh International Symposium on Ferrocement and Thin Reinforced Cement Composites, National University of Singapore, 27-29, pp 465- 471, June 2001.

Effect of relative proportion of pozzolana on compressive strength of concrete under different curing conditions

Shweta Goyal

Lecturer/Civil Engineering Department
Thapar University
Patiala, 147004, India

shweta@tiet.ac.in

Maneek Kumar

Professor/Civil Engineering Department
Thapar University
Patiala, 147004, India

maneek@thapar.edu

B. Bhattacharjee

Professor/Civil Engineering Department
IIT Delhi
New Delhi, India

bishwa@civil.iitd.ac.in

Abstract

In this experimental and analytic research, the effect of curing regime on various combinations of silica fume and fly ash was investigated in terms of development of compressive strength. Over 24 mixes were prepared with the water-to-binder ratios of 0.45, 0.35 and 0.25 and with differing percentage of additives used as a combination of 2 or 3 binders. The specimens were subjected to five different curing regimes ranging from continuously water cured to continuously air cured. Results show that it is economical to use a combination of silica fume and fly ash rather than using only silica fume for attaining the same strength level. Poor curing condition adversely affect the strength characteristics of pozzolanic concrete than that of OPC concrete. For silica fume concrete, it is necessary to apply water curing for the initial 7 days to explore pozzolanic activity but it is imperative to cure the fly ash concrete for an extended period to utilize its full potential.

Keywords: strength, curing, ternary, silica fume, fly ash

1. INTRODUCTION

Mineral admixture concrete is one of the most significant new material available worldwide for new construction and for rehabilitation purposes. Studies have shown [1 –4] that mineral admixtures such as blast furnace slag, fly ash and silica fume enhance the strength and durability of concrete. Research concerning the use of mineral admixtures to augment the properties of concrete has been going on for many years. Economics (lower cement requirement) and environmental considerations also have a role in the growth of mineral admixture usage. The

lower cement requirement leads to a reduction in the amount of carbon dioxide generated by the production of cement and hence its emission to atmosphere [5, 6].

The addition of wide range of blending material also introduces significant diversity into the cementing system. For instance, addition of silica fume increases early strength of concrete by formation of secondary C-S-H at early stages due to fast pozzolanic reaction [7 – 9]. However, it decreases the flowability of fresh concrete due to its very fine particles and hence the properties of silica fume can be enhanced by the presence of superplasticizers in the mix [6]. Unlike silica fume, fly ash mixes require longer period of time to develop strength [10]. At 28 days, the degree of fly ash reaction rate is slightly more than 10 percent [11 – 14]. However, fly ash leads to workability enhancement due to its spherical particles that easily roll over one another reducing inter particle friction (called ball bearing effect) [15]. In India, silica fume comes under the category of costly materials and fly ash is abundantly available worldwide and its production is ever increasing. Therefore, a combination of silica fume and fly ash can be a better option in terms of modifying the properties (fresh and hardened) of resultant concrete and in terms of economy.

Over the past several decades, numerous failures of concrete structures during construction due to accelerated construction schedules have emphasized the early age strength gain of concrete [16] and importance of minimum days of curing for concrete [17]. In the standards, the minimum curing periods under certain weather conditions are specified. For most of the structures, initial moist curing for 7 days is essential [19]. The reported longer curing period required for blended cement concretes, as opposed to plain cement concrete, is still a question often debated among concrete technologists. Since pozzolanic reaction is highly dependent on good curing practice, there is often concern as to the effect of curing for pozzolanic cement concrete. Many investigators [19 – 21] believe that a curing period of about 28 to 90 days is required for pozzolanic cement concrete specimens to attain properties superior to that of plain cement concrete. However, not much research has been carried out on strength development characteristics of ternary mixes containing a combination of OPC – silica fume and fly ash.

This research is intended to expand the knowledge concerning the relative performance of a range of mixes made with OPC, silica fume and fly ash either as binary or ternary combinations. The performance evaluation has been carried out in terms of mechanical properties which include compressive strength, tensile strength and permeability under five different curing conditions. Based on the test results, the effect of relative percentage of ingredients, water – binder ratio and curing condition has been discussed. Also, the effect of wet – dry cycling condition on the deterioration mechanism of short-term cured concrete is studied.

2. EXPERIMENTAL PROGRAM

2.1. Materials:

2.1.1. Cementitious material: ASTM Type I Portland cement is used in this study. Its chemical composition is given in Table 1. The chemical and physical characteristics of two mineral admixtures silica fume and fly ash are also given in Table 1.

2.1.2. Aggregates: Crushed granite with a maximum nominal size of 10 mm was used as coarse aggregate and natural riverbed sand conforming to Zone II with a fineness modulus of 2.52 was used as fine aggregate. The properties of aggregates are listed in Table 2.

2.1.3. Super-plasticizer: Polycarboxylic group based superplasticizer, Structro 100 (a product of Fosroc chemicals), is used throughout the investigation. This group maintains the electrostatic charge on the cement particles and prevents flocculation by adsorption on the surface of cement particles [22]. It is a light yellow coloured liquid complying with requirements of IS 9103 – 79, BS 5075 Part III and ASTM – C494 Type F. The specific gravity of superplasticiser is 1.2 and solid content is 40 percent by mass.

1 Table 1: Physical, chemical and strength characteristics of cement

Characteristic	OPC	SF	FA
Physical Tests			
Normal Consistency (%)	32		
Vicat (hour: minute)			
Initial	2:10		
Final	4:08		
Specific Gravity	3.12		2.42
Le-Chatelier (mm)	1.5		
Fineness (% retained on 90 micron sieve)	3.2		
Particle shape	Angular	Spherical	Spherical
Mean particle diameter (μm)		19.6	0.1
Chemical			
CaO(%)	61.7	0.5	1.7
SiO ₂ (%)	22.4	90.7	56.8
Al ₂ O ₃ (%)	5.93	0.68	25.8
Fe ₂ O ₃ (%)	4.91	2.2	6.43
SO ₃ (%)	2.28		1.4
MgO(%)	1.5	1.47	0.6
K ₂ O(%)	0.65	0.9	0.79
Na ₂ O(%)	0.122	0.86	0.36
Loss on ignition(%)	1.27	2.5	2.15
Insoluble Residue(%)	4.52		84.9
Blaine fineness (m ² /kg)	287.8	19.7	
Density (kg/m ³)	3150	650	
Accelerated pozzolanic activity index (7 days) %		98	
Strength			
f _c (3 days) (MPa)	26.5		
f _c (7 days) (MPa)	36.2		
f _c (28 days) (MPa)	47.3		

Table 2: Properties of aggregates

Property	2 FA	3 CA
Unit mass (kg/m ³)	1.692	1.68
Specific gravity	2.54	2.64
Percentage absorption (%)	1.95	1.12
Sieve Analysis	Cumulative percentage retained (%)	
20mm	0	0
10 mm	0	2.5
4.75 mm	5.05	92.8
2.36 mm	9.55	98.6
1.18 mm	17.6	100
600 μ	44.6	100
300 μ	80.15	100

2.2. Specimen Details and Preparations:

Three series of concretes were produced in this study corresponding to three water-to-binder ratios: 0.45, 0.35 and 0.25 to ensure wide variation of strength. For each series, eight separate batches were prepared: one control, 3 mixes containing different percentage of silica fume and fly ash and 4 made of combinations of silica fume and fly ash. The slump of the fresh concrete was kept in the range of 200 \pm 20 mm. A pre-study was carried out to determine the optimum superplasticizer dosage for achieving the desired workability based on the slump cone test ASTM C 143 – 90 (a) [23]. The mix details of specimens are listed in Table 3 and Table 4. Mixing water was adjusted to correct for aggregate absorption and for the additional water brought into mix from superplasticizers.

Table 3: Mix proportions for control mixes

Water binder ratio	Mix proportions (kg/m ³)			Water	Mix Ratio
	Cement	F.A.	C.A.		
0.25	520	521.1	1340.4	130	1:1.042:2.681
0.35	457.1	523.9	1283	160	1:1.146:2.807
0.45	422.2	556.8	1183.3	190	1:1.319:2.802

Table 4: Details of mixes

Mix type	Notation	W/B	OPC (%)	Mineral admixture (% replacement of OPC)		Superplasticizer dosage (wt. of binder)
				SF	FA	
Control mixes	M1	0.25	100	-	-	4
	M2	0.35	100	-	-	1.25
	M3	0.45	100	-	-	0.2
Binary mixes	M1BS1	0.25	95	5	-	3.75
	M1BS2	0.25	90	10	-	4.25
	M1BF1	0.25	70	-	30	2
	M2BS1	0.35	95	5	-	1.5
	M2BS2	0.35	90	10	-	2
	M2BF1	0.35	70	-	30	0.5
	M3BS1	0.45	95	5	-	0.3
	M3BS2	0.45	90	10	-	0.7
	M3BF1	0.45	70	-	30	0.1
	Ternary mixes	M1TC1	0.25	80	5	15
M1TC2		0.25	75	5	20	2.75
M1TC3		0.25	75	10	15	3.5
M1TC4		0.25	70	10	20	3.25
M2TC1		0.35	80	5	15	1
M2TC2		0.35	75	5	20	0.75
M2TC3		0.35	75	10	15	1.5
M2TC4		0.35	70	10	20	1.25
M3TC1		0.45	80	5	15	0.1
M3TC2		0.45	75	5	20	0.1
M3TC3		0.45	75	10	15	0.4
M3TC4		0.45	70	10	20	0.3

2.3. Testing procedure:

Concrete batches were mixed in a pan mixer for 3 minutes. $150 \times 150 \times 150$ – mm³ cubes were cast for the compressive strength tests. The specimens were cast in accordance with ASTM C 192 – 88 [24]. Plastic sheets were used to cover the specimens to prevent water from evaporating. After 24 hours, the specimens were stripped from their respective molds and the curing regime as given in Table 5 was applied. The strength tests were carried out at 1, 3, 7, 14, 28, 56, 90 days taking the average of six specimens for each test. In the case of mixes prepared at water binder ratio of 0.25, the specimens were stripped off after 36 hours and therefore, the compressive strength studies were started at the end of 2 days instead of 1 day. The test procedure followed during the test was in conformity with BS 1881:Part 116:1983 [25]

Table 5: Summary of curing regimes adopted

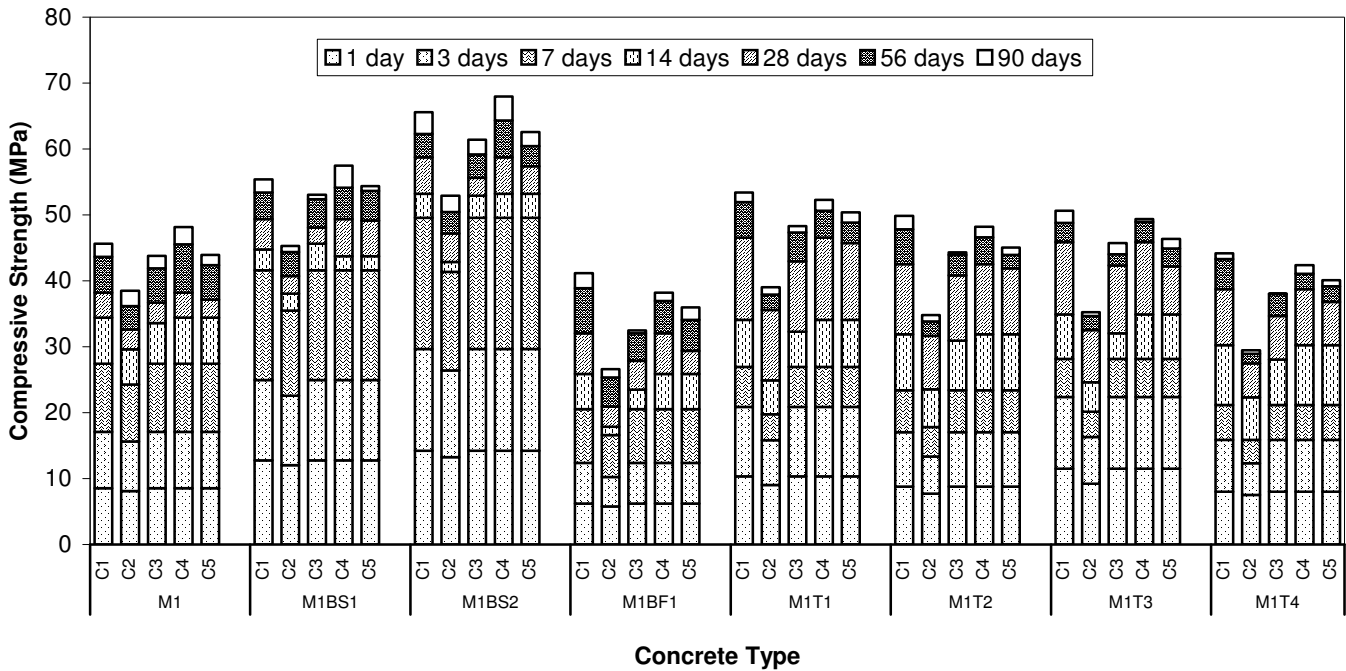
Curing Regime	Description
1.	Continuously water curing at temperature of $25 \pm 2^\circ\text{C}$
2.	Continuously air curing in the lab environment at around $25 \pm 5^\circ\text{C}$ and $50 \pm 10\%$ RH
3.	Initial 7 days of water curing followed by air drying (as in No. 2)
4.	Initial 28 days of water curing followed by air drying (as in No. 2)
5.	Initial 14 days of water curing followed by wetting and drying cycles of 7 days duration

3. RESULTS AND DISCUSSIONS

3.1 Compressive strength results

The compressive strength development is illustrated in Figs. 1 (a to c) for water binder ratios of 0.45, 0.35 and 0.25 respectively.

(a) water binder ratio: 0.45



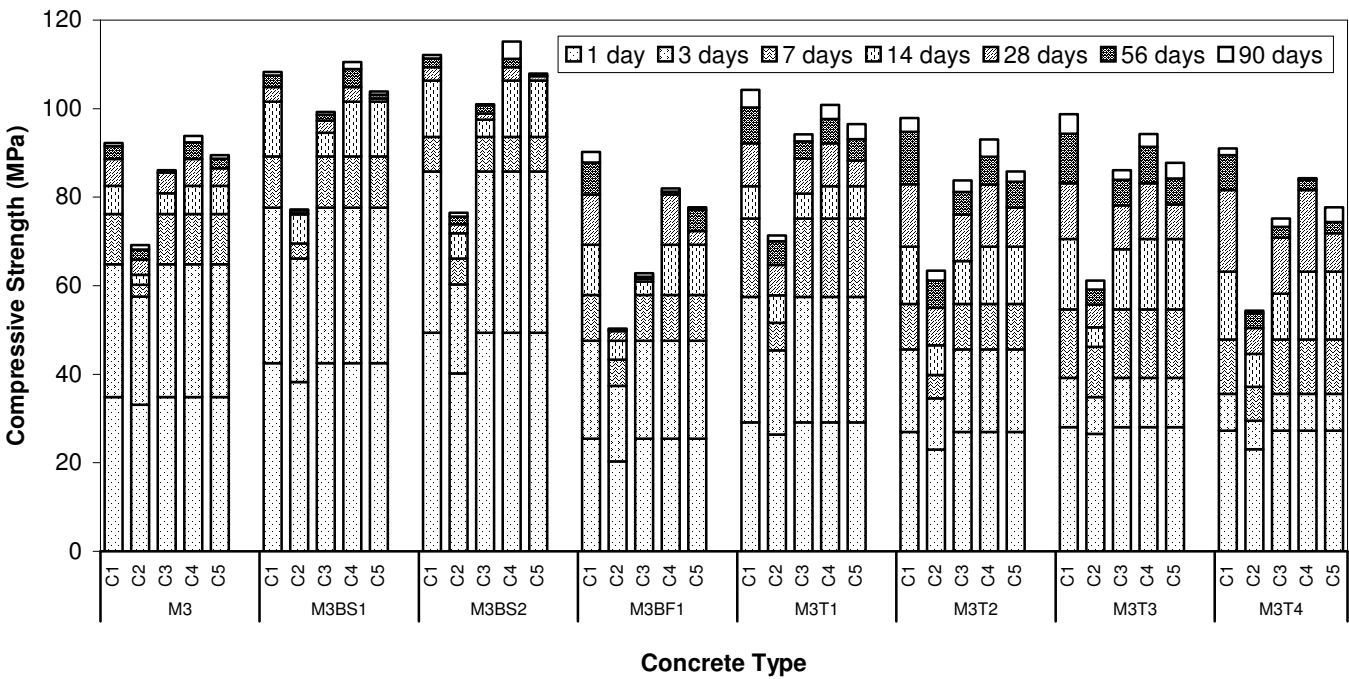
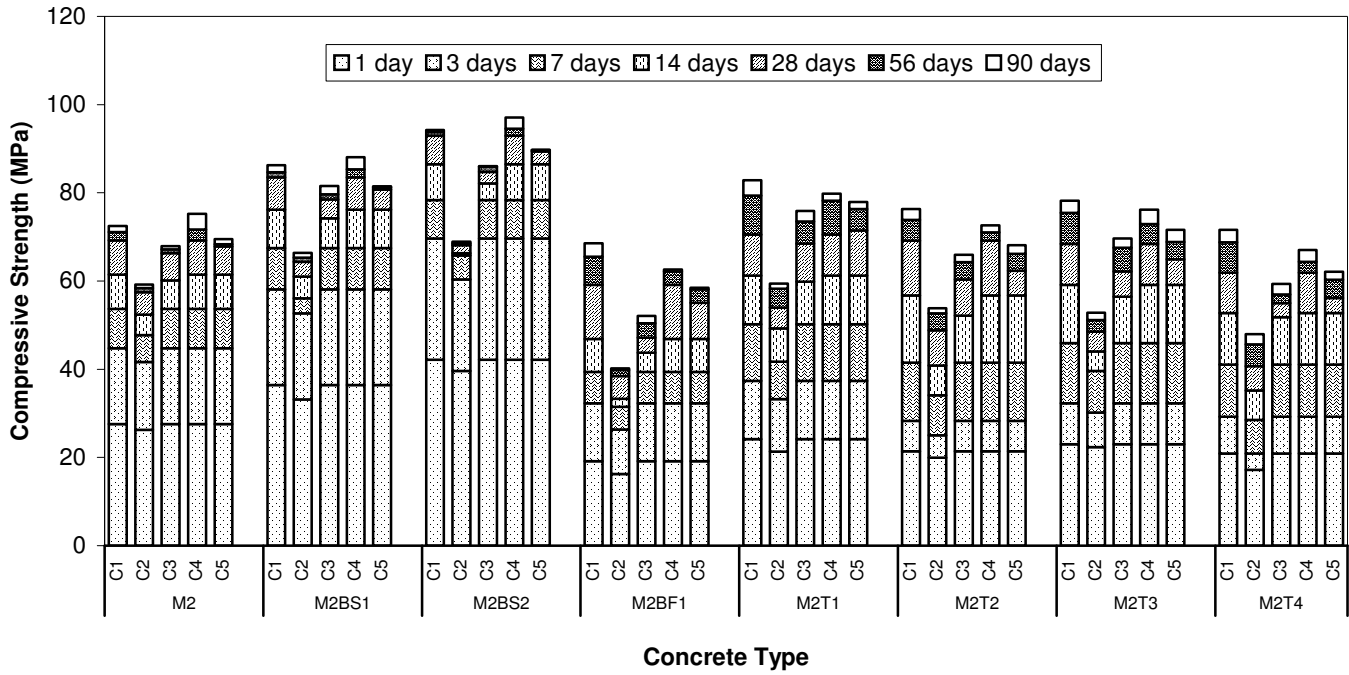
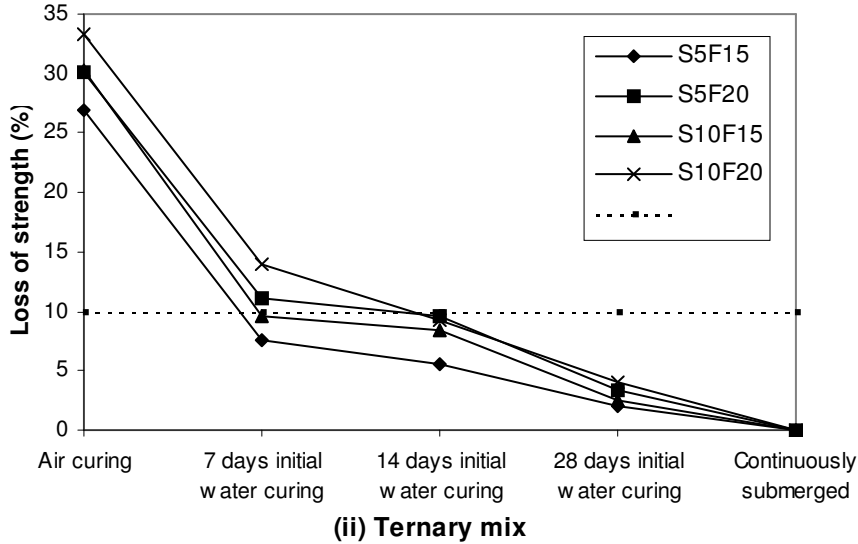


Fig. 1 Variation of compressive strength development of plain and blended concrete

3.1.1. Effect of supplementary cementitious materials

The addition of silica fume produced the increase in strength while addition of fly ash produced



decrease in strength for all water-to-binder ratios. The better performance of silica fume concrete could be attributed to the improvement in the bond between the hydrated cement matrix and aggregate. This is due to the combined effect of secondary pozzolanic reaction and extremely fine silica fume particles [27, 28]. Among silica fume concrete mixes also, the compressive strength increases as the percentage replacement is increased from 5% to 10%.

The combination of silica fume and fly ash leads to increase in compressive strength as compared to control mix at all water binder ratios. The combination of 5% silica fume, 15% fly ash and 80% cement performed best among the four combinations studied and produced an increase in strength of about 17%, 12.5% and 13.3% respectively at water binder ratios of 0.45, 0.35 and 0.25 over the control mix. This combination produced strength almost similar to the strength of mix having 5% silica fume and 95% cement.

3.1.2. Effect of curing regime

In Fig. 1, it is common that air cured specimens gained the lowest strength for all mixes and at all ages. In general, compressive strength of concrete increased with increase in initial water curing period. This general trend has some exceptions in the case of OPC and silica fume concrete mixes. These mixes exhibit higher strengths at 56 and 90 days when initially water cured for 28 days (C4 curing condition) as compared to continuously submerged specimens (C1 curing condition). The higher strength of partial dried specimens can be attributed to the increase in secondary forces between the surfaces of cement gel [26, 31] and also to the reduction in disjoining pressure due to drying [17].

The average difference between compressive strength at two extreme curing conditions, continuously air cured and continuously water cured, is smaller for OPC concretes than those for pozzolanic concretes showing that mineral admixture concrete is more sensitive to inadequate curing than OPC concrete, as indicated previously [17, 32]. This can be attributed to the lack of development of hydration and pozzolanic reactions to produce a dense microstructure and the extensive shrinkage cracking which may have developed due to air curing as is indicated by other researchers [33, 34].

In order to find the days of initial water curing that is both necessary and sufficient for all mixes, percentage loss of strength under the given curing condition with reference to the submerged condition at 90 days is plotted against the initial curing period (Figs. 2 to 4). From the Figs. 2 to 4, it is clear that continuous air curing leads to very high loss of strength and should never be considered as a curing practice. Also, if 7 days of initial curing practice is adopted, then binary

mixes with silica fume and ternary mixes (T1 and T3) are able to reach 90% of strength of continuously water cured specimens. It can be concluded that 7 days of initial water curing is sufficient to explore the pozzolanic activity for these mixes.

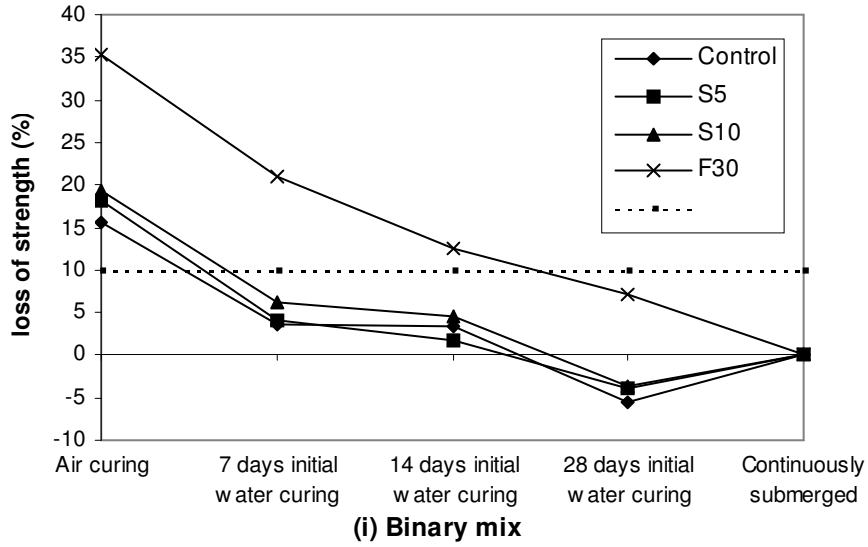
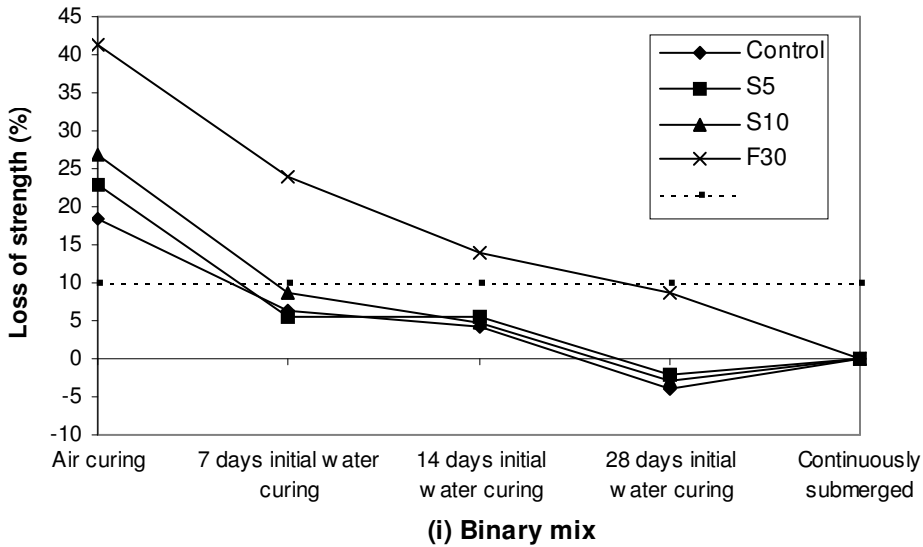


Fig. 2 Percentage loss of mixes compared to continuously submerged condition at water binder ratio of 0.35.



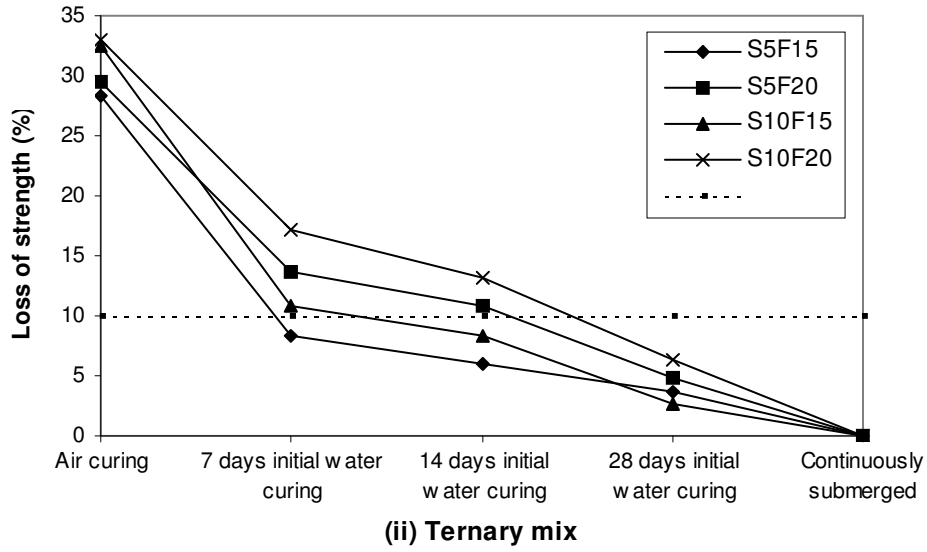
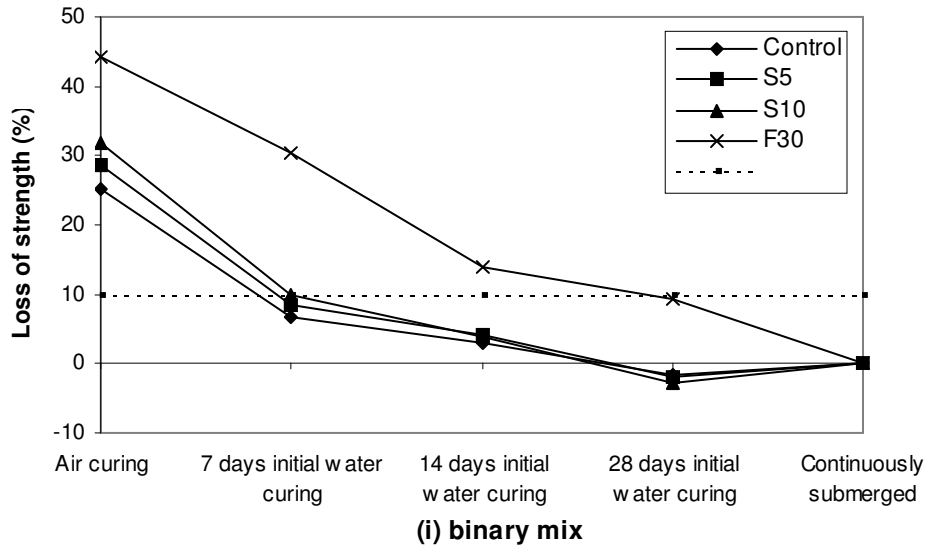


Fig. 3 Percentage loss of mixes compared to continuously submerged condition at water binder ratio of 0.35.



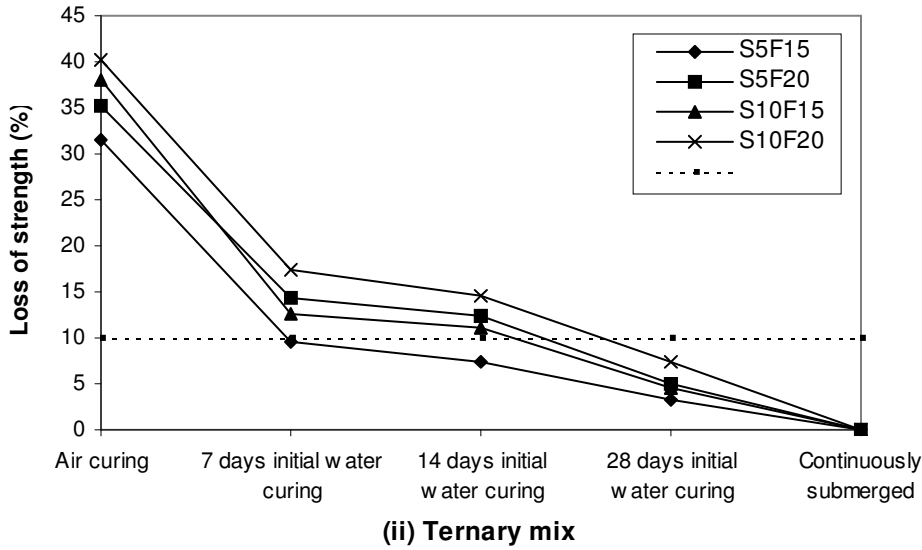


Fig. 4 Percentage loss of mixes compared to continuously submerged condition at water binder ratio of 0.25.

The strength development of mixes was further analyzed by using the equation:

$$f_c = aLn(t)+b$$

where f_c is the compressive strength of concrete at t days, a and b are constants. The constants a and b are obtained from least square method and are given in Table 6. The correlation coefficients are quite high (mostly > 0.95) for almost all the mixes.

In this equation, constant a represents the strength gaining rate of concrete. From the table, it seems that the strength-gaining rate is less sensitive to initial water curing at higher water binder ratios and becomes more and more sensitive as the water binder ratio is decreased. Also, the strength – gaining rate is sensitive for mixes containing fly ash confirming that fly ash concrete is more affected by the curing practice adopted.

Mix Type	Control		BS1		BS2		BF1	
Regression constants	a	b	a	b	a	b	a	b
Curing Regime	Water-to-binder ratio = 0.45							
R1	8.51	9.38	9.5	16.5	11.28	19.23	8.13	4.93
R2	6.85	9.23	7.35	15.65	8.55	17.77	4.69	5.86
R3	8.02	9.76	9.03	17.11	10.28	20.32	6.1	6.84
R4	9.02	8.73	9.83	15.92	11.79	18.69	7.56	5.65
R5	8.11	9.8	9.37	16.53	10.64	20.04	6.85	6.32

	Water-to-binder ratio = 0.45							
R1	9.99	32.13	10.84	43.19	10.99	52.12	11.29	18.97
R2	7.05	31.32	6.69	40.23	5.5	48.75	5.22	19.18
R3	8.86	33.16	9.46	44.27	8.7	53.78	7.05	22.93
R4	10.4	31.58	11.13	42.81	11.41	51.55	10.2	20.36
R5	9.27	32.93	9.75	44.36	9.82	53.31	9.06	21.47
	Water-to-binder ratio = 0.45							
R1	12.59	43.03	14.42	52.65	13.76	60.35	15.84	24.28
R2	7.05	41.12	7.61	48.85	7.78	46.06	6.44	25.87
R3	10.85	45.21	11.58	55.4	9.94	63.66	7.64	34.15
R4	12.92	42.51	14.92	51.87	13.91	59.59	13.83	27.37
R5	11.72	44.19	13.1	54.45	12.28	62	12.25	29.14

Table 6: Strength development constants of control and binary mixes

Mix Type	TC1		TC2		TC3		TC4	
Regression constants	a	b	a	b	a	b	a	b
Curing Regime	Water-to-binder ratio = 0.45							
R1	10.14	9.43	9.78	7.1	9.08	11.83	8.7	6.96
R2	7.2	7.94	6.55	6.83	6.15	9.25	5.34	7.17
R3	8.84	10.56	8.59	8.35	7.78	9.25	7.17	8.29
R4	9.87	9.76	9.45	7.52	8.93	12.04	8.26	7.51
R5	9.4	10.3	8.75	8.34	7.96	12.95	7.68	8.09
	Water-to-binder ratio = 0.45							
R1	13.54	24	13.64	18.26	13.23	21.47	12.13	19.06
R2	8.63	23.69	8.26	18.6	6.96	23.79	7.37	15.23
R3	11.95	25.66	10.87	20.45	11.01	23.41	9.03	22.27

R4	13.04	24.66	12.89	19.21	12.72	22.09	11.11	20.32
R5	12.66	25.21	11.48	20.44	11.56	23.28	9.78	21.56
Water-to-binder ratio = 0.45								
R1	17.4	31.92	18.02	20.57	18.8	17.95	17.9	15.64
R2	10.47	28.05	10.09	19.92	8.68	25.13	8.37	20.04
R3	14.8	35.43	13.94	25.82	15.4	22.45	13.01	21.53
R4	16.59	33.18	16.65	22.64	17.78	19.53	16.24	18.2
R5	15.2	35	14.61	25.37	15.72	22.29	13.59	21.39

Table 7: Strength development constants of ternary mixes

4. CONCLUSION

The present research focused on studying the effect of silica fume and fly ash either in binary mix or in ternary mix on strength of concrete and to determine how curing conditions affects concrete strength. Based on the results obtained the following conclusions can be drawn:

1. Specifying concrete on the basis of 28 days compressive strength under estimates the general beneficial effects of mineral admixture concrete. Water binder ratio, cement type, age and curing conditions have significant effect on strength characteristics of concrete.
2. It is economic to use a combination of silica fume and fly ash rather than using only silica fume as mineral admixture for attaining the same strength level. Among the ternary mixes, Mix T1, with a combination of 5% silica fume and 15% fly ash, showed the highest increase in strength for the entire range of water binder ratios. Using T1 mix leads to 10 to 15% cost saving as compared to mix with 5% silica fume and no fly ash.
3. Continuous air curing is worst curing regime for all mixes. Although, the curing conditions affect the strength of both OPC concrete and mineral admixture concrete, however, pozzolanic concretes are more adversely affected by poor curing practices than OPC concrete. For totally submerged curing condition, strength gaining rates of OPC concrete is lower than mineral admixture concrete. However, the trend becomes opposite for air curing condition.
4. For silica fume concrete and for a ternary combination that has lesser amount of fly ash in it, 7 days of initial water curing is both necessary and sufficient to explore the pozzolanic activity. However, for mixes having larger percentage of fly ash, a long initial moist curing period is necessary to fully benefit from the addition of these supplementary cementitious materials. Replacing cement by percentage greater than 20% tends to lower the efficiency of mineral admixtures. At this replacement level, the pozzolanic reaction start becoming lime controlled instead of being pozzolana controlled. If the percentage replacement of cement reaches 30%, the strength of resultant mix is even lesser than the corresponding control mix.

Acknowledgements

This research is supported by The Department of Science and Technology Grant No. 92780. The authors would like to acknowledge the authorities concerned for its assistance in carrying out the research.

5. REFERENCES

1. Bouzoubaa N, Fournier B, Malhotra V M, Golden D. Mechanical properties and durability of concrete made with high volume fly ash blended cement produced in cement plant. *ACI Materials Journal*, 99, (6), 2002, 560 – 567.
2. Mazloom M, Ramezani-pour A A, Brooks J J. Effect of silica fume on mechanical properties of high strength concrete. *Cement and Concrete Composites*, 26, 2004, 347 – 357.
3. Tan K, Pu X. Strengthening effects of finely ground fly ash, granulated blast furnace slag, and their combination. *Cement and Concrete Research*, 28, (12), 1998, 1819 – 1825.
4. Ozyildirim C, Halstead WJ. Improved concrete quality with combination of silica fume and fly ash. *ACI materials Journal*, 1994, 91 (6), 587 – 594.
5. Ferraris C F, Obla K H, Hill R. The influence of mineral admixtures on the rheology of cement paste and concrete. *Cement and Concrete Research*, 31, 2001, 245 – 255.
6. Toutanji H, Delatte N, Aggoun S, Duval R, Danson A. Effect of supplementary cementitious materials on compressive strength and durability of short term cured concrete. *Cement and Concrete Research*, 34, 2004, 311 – 319
7. Duval R. and Kadri E.H. Influence of silica fume on the workability and compressive strength of high performance concrete. *Cement and Concrete Research*, 28, (4), 1998, 533 – 547.
8. Zhang X, Han J. The effect of ultra-fine admixture on the rheological property of cement paste. *Cement and Concrete Research*, 30, (5), 2000, 827 – 830.
9. Bagel, L. Strength and pore structure of Ternary Blended Cement Mortars Containing Blast Furnace Slag and Silica Fume. *Cement and Concrete Research*, Vol. 28, No. 7, 1998, 1011 – 1020.
10. Langley W S, Carette G G, Malhotra V M, 'Structural concrete incorporating high volume ASTM Class F fly ash', *ACI Materials Journal*, 86, (1989), 507 – 514.
11. Poon C S, Lam L, Wong Y L. A study on high-strength concrete prepared with large volumes of low calcium fly ash. *Cement and Concrete Research*, 30, (3), 2000, 447 – 455.
12. Lam L, Wong Y L, Poon C S. Degree of hydration and gel/space ratio of high-volume fly ash/cement systems. *Cement and Concrete Research*. 30, (5), 2000, 747 – 756.
13. Chen Y, Li D, Shen J, Su J, Wu X. The influence of alkalinity on activation and microstructure of fly ash. *Cement and Concrete Research*, 30, (6), 2000, 881 – 886.
14. Fu X, Hou W, Yang C, Li D, Wu X. Studies on high-strength slag and fly ash compound cement. *Cement and Concrete Research*, 30, (8), 2000, 1239 – 1243.
15. Gopalan M K. Nucleation and pozzolanic factors in strength development of class F fly ash concrete. *ACI materials Journal*, 90, (2), 1993, 117 – 120.
16. Kim J K, Moon Y H, Eo S H. Compressive strength development of concrete with different curing time and temperature. *Cement and Concrete Research*, 28, (12), 1998, 1761 – 1773.
17. Ozer B and Qzkul M H. The influence of initial water curing on the strength development of ordinary Portland and pozzolanic cement concretes. *Cement and Concrete Research*, 2006, 1 – 6.
18. Manmohan D, Mehta P K. Influence of pozzolanic slag and chemical admixtures on pore-size distribution and permeability of hardened cement pastes. *Cement, Concrete Aggregates*, 3, (1), 1981, 63 – 67.
19. Nagataki S, Ujike I I. Air permeability of concretes mixed with fly ash and condensed silica fume. *International proceedings 2nd International Conference on the use of fly ash, blast furnace slag and silica fume concrete*. Madrid, 1986, 1049 – 1068.
20. Marsh B K, Day R L, Bonner D G. Pore structure characteristics affecting the permeability of cement paste containing fly ash. *Cement and Concrete Research*, 15, 1985, 1027 – 1038.
21. Mitsui, K. et al. Properties of High strength concrete with silica fume using high – range water reducer and other Chemical Admixtures in Concrete, Ed. V.M. Malhotra, *ACI SP – 119*, 1989, 79 – 97.
22. ASTM Designation C 143 – 90a, Standard test method for slump of Portland cement concrete, 1994.
23. ASTM Designation C 192 – 90a. Standard Practice for Making and Curing Concrete Test Specimens in the Laboratory, 1994.

24. BS Designation 1881: Part 116. Method for Determination of Compressive Strength of Concrete Cubes, 1983.
25. Popovics S. Effect of curing method and final moisture condition on compressive strength of concrete. *ACI Journal*, 83 (4), 1986, 650 – 657.
26. Hassan K E, Cabrera J G and Maliehe R S. The effect of mineral admixtures on the properties of high performance concrete. *Concrete Composites*, 22, 2000, 267 – 271.
27. Jaturapitakkul C, Kiattikomol K, Sata V and Leekeeratikul T. Use of ground coarse fly ash as a replacement of condensed silica fume in producing high strength concrete. *Cement and Concrete Research*, 34, 2004, 549 – 555.
28. Langan B W, Weng K and Ward M A. Effect of silica fume and fly ash on heat of hydration of Portland cement. *Cement and Concrete Research*, 32, 2002, 1045 – 1051.
29. Neville, A.M. and Brooks, J.J. *Concrete Technology*. ELBS Edition Produced by Longman Singapore Publishers, (Pte). Ltd. 1990
30. Tan K, Gjorv O E. Performance of concrete under different curing conditions. *Cement and Concrete Research*, 26, 3, 1996, 355 – 361.
31. Ramezaniapour A A and Malhotra V M. Effect of curing on compressive strength, resistance to chloride ion penetration and porosity of concrete incorporating slag, fly ash or silica fume. *Cement and Concrete Composites*, 17, 2, 1995, 125 – 133.
32. Toutanji H A and Bayasi Z. Effect of curing procedures on properties of silica fume concrete. *Cement and Concrete research*, 29, 1999, 497 – 501.
33. Lam L, Wong Y L, Poon C S. Effect of fly ash and silica fume on compressive and fracture behaviour of concrete. *Cement and Concrete Research*, 28, 2, 1998 271 – 283.
34. Yurtdas I, Peng H, Burlion N, Skoczylas F. Influence of water to cement ratio on mechanical properties of mortars submitted to drying. *Cement and Concrete Research*, 36, 2006, 1286 – 1293.

ELECTROSTATIC AND ELECTROMAGNETIC FIELDS ACTUATORS FOR MEMS AD/DA CONVERTERS

Amir J. Majid; *Associate Prof.*
Faculty of Engineering,
Ajman University of S&T
Ajman, U.A.E.

abac.majid.a@ajman.ac.ae

Abstract

MEMS Analog -to-digital and digital-to- analog converters are proposed using electrostatic field and electromagnetic fields actuators. For the former, parallel deformable plates supported by springs are used with bias applied voltage which determines the amount of static displacement needed for equilibrium condition. For the latter, coil winding(s) are embedded in a rotating plate, which is exposed to a constant field of a permanent magnet, causing the plate to deflect according to the currents in the windings. In the analog-to-digital arrangement, different spring displacements are tapped off either the spring in case of electrostatic or the moving plate in case of electromagnetic actuators, corresponding to the binary decoded currents. At these off tapping points, logic high signal levels are applied at these locations so that when a certain analog voltage is applied on the moving plate of the capacitor, the spring is displaced to one of these locations, enabling different binary voltages to all switches up to that level. Similar result occurs when an analog voltage is applied on the winding. The digital binary voltages are fed to a priority encoder to obtain the digital value. In digital-to-analog arrangement, the input binary voltage is decoded to different spring locations which correspond to resistances making up a potentiometer circuit for the output analog voltage. Similarly; for the electromagnetic actuator, a number of different length coil windings are embedded within the moving plate, causing different deflections corresponding to one bit of the binary input.

Keywords: ADC, DAC, MEMS, Electrostatic, Electromagnetic

1. INTRODUCTION

1.1 Electrostatic field actuator

The parallel plate capacitor with one movable plate supported by a mechanical spring is depicted in Figure (1), where the top plate is supported by a spring with the force constant being K_m . At rest the applied voltage, displacement and the mechanical restoring forces are zero. Gravity does not play an important role in the static analysis of micro devices because the mass of plates is generally very small and the gravitational force would not cause appreciable static displacement.

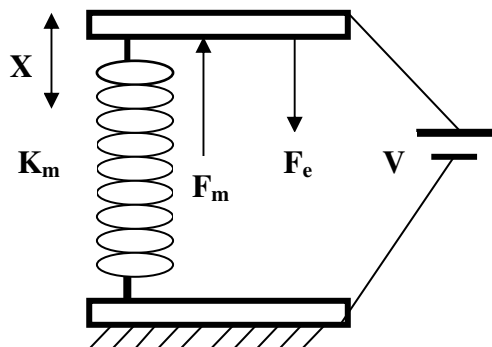


FIGURE 1: A Coupled Electromechanical Model

When a voltage is applied an electrostatic force F_e will be developed with a magnitude of

$$F_e = \epsilon A V^2 / [2 d^2]$$

with the movable plate is at its starting position. This force tends to decrease the gap which gives rise to displacement and the mechanical restoring force. Under static equilibrium the mechanical restoring force has an equal magnitude but opposite direction as the electrostatic force. The magnitude of the electrostatic force is itself a function of the displacement. It's to be noted too that this electrostatic force affects the spring constant as well, due to the spring being softer due to this force. The spatial gradient of the electric force is defined as an electrical spring constant

$$K_e = \Delta F_e / \Delta d = CV^2 / d^2$$

As seen the magnitude of electric spring constant changes with position d and the biasing voltage V . This is ignored for small displacements. Thus the effective spring constant is mechanical spring constant minus the electrical spring constant.

To derive the equilibrium displacement of a spring supported electrode plate under a bias voltage V , consider the resulting equilibrium displacement being x in the direction of increasing gap. With displacement x , the gap between the two electrode plates is $d+x$ and thus the electrostatic force at equilibrium is

$$F_e = \epsilon A V^2 / [2 (X_0 + X)^2] = C(X) V^2 / [2 (X_0 + X)]$$

Whereas the mechanical force is $F_m = -K_m X$

By equating these two forces, and rearranging terms,

$$X = F_m / K_m = F_e / K_m = C(x) V^2 / [2 (X_0 + X) K_m]$$

The displacement at equilibrium can be calculated from the above quadratic equation as shown. This can be visualized graphically as shown in Figure (2). The horizontal axis represents space between the two plates, and the vertical axis is the mechanical or electrical force irrespective to their directions. The movable plate is displaced X_0 from the rigid fixed plate at origin. Two curves representing both mechanical and electrical forces are plotted with electrode positions according to their quoted equations and their intersecting points correspond to the solutions of the above quadratic equation. It can be noted that more than one intersecting points exist, but only one is achieved in reality. The solution that is closest to the rest position is realized first and is generally the realistic solution.

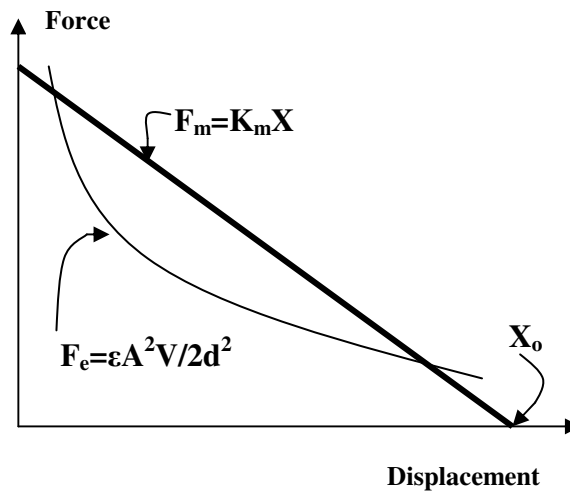


FIGURE 2: Electrical and Mechanical Forces as Functions of Spring Displacement

The graphic solution can be used to track the equilibrium position as the bias voltage is increased. As the voltage increases, the family of curves corresponding to electrostatic force shifts upwards, shifting the x coordinates of the interception points further away from the rest position.

1.2 Electromagnetic field actuator

A moving coil electromagnetic capable of one-axis rotation is proposed as depicted in Figure (3). A plate is supported by torsional hinge structure of embedded conducting wires, constituting multi windings positioned at different locations. The conducting wires of these windings are therefore of different lengths. Two permanent magnets are placed on the side of the plate, such that the magnetic field lines are parallel to the plane and orthogonal to the torsional hinges.

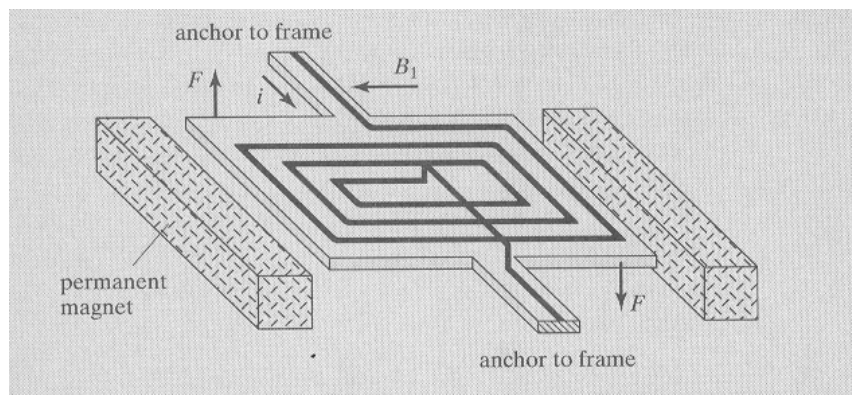


FIGURE 3: Electromagnetic field actuator

When current passes through the coils, Lorentz forces will develop and cause rotational torque on the plate. The direction of the torque depends on the direction of input currents. The magnitude of torque acting on this actuator is:

$$T = i B l_1 l_2 N$$

where i is the winding current, B is the magnetic field density, l_1 & l_2 are the length and width of the coil and N is the number of turns per winding.

Since torque is linearly proportional with both winding current and winding turn length & width, different geometrical dimensions will give different resonant frequencies and thus different rotational angles for the same input current.

2. PULL-IN VOLTAGE

At a particular bias voltage the two curves intercept at one point tangentially as shown in Figure (4). At this interception point the electrostatic and mechanical force balance each other. At this point, the magnitude of electric and mechanical spring constants is equal. This is given by the gradient of the electrostatic force curve at the interception point, making the effective spring constant equal to zero, i.e. extremely soft. The bias voltage that invokes this condition is called the pull-in voltage V_p .

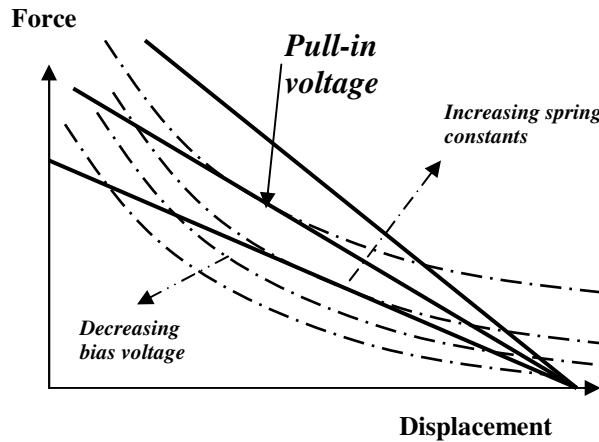


FIGURE 4: Balance of Electrical and Mechanical Forces at Different Bias Voltages And Different Spring Constants

This pull-in voltage can be calculated as

$$V^2 = -2k_m X(X+X_0)^2 / [\epsilon A] = -2k_m X(X+X_0)/C$$

The value of x is negative when the spacing between the electrodes decreases.

If the bias voltage is increased further beyond V_p the two curves will not intercept and no equilibrium solution exists. In reality the electrostatic force continues to grow while the mechanical force is unable to catch up and match it. The two plates are thus pulled against each other rapidly until they contact, at which the mechanical force will finally balance the electric one. This is termed as the pull in or snap in condition. Now substituting the pull in voltage in the electric force constant equation $K_e = CV^2/d^2$ yields

$$K_e = CV^2/[X+X_0]^2 = -2K_m X/[X+X_0]$$

The only solution in which $K_e = K_m$ is when $x = -X_0/3$.

This states that the relative displacement of the plates from its rest position is one third of the original spacing at the critical pull-in voltage irrespective of the actual mechanical force constant or actual pull-in voltage value. Substituting this displacement in the pull-in voltage equation yields

$$V_p^2 = 4X_o^2 K_m/9C$$

or $V_p = 2X_o/3 [K_m/1.5 C_o]^{1/2}$

3. ELECTROSTATIC ADC

The electrostatic field force within two plated capacitor is used to move the spring contacts at 8 different locations according to the pull-in voltages found from Figure (5), each one is a multiple of the previous contacts ones. This constitutes the binary digital values. Once connected, these contacts apply a zero voltage on a PMOS switch, thus continuing the circuit to the next contact and finally to the reference high voltage. This is depicted in Figure (5), which also shows the use of 7-3 priority encoder converting the contacts tapped voltages to binary digital voltage. Table (1) lists the truth table of the encoder.

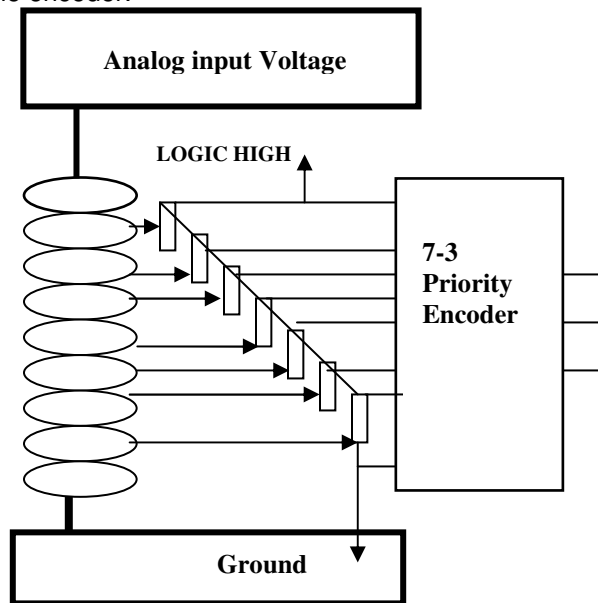


FIGURE 5: ADC using 7 PMOS switches at spring taps and an 7-3 priority encoder

4. ELECTROSTATIC DAC

In a similar manner, the two plated capacitor is used with a decoder and a spring operated potentiometer to implement a DAC. In this case a 3-8 decoder is used to energize one output at a time. This output is spring position switch which enables a current source to flow in the spring resistance thus dropping an output voltage according to $I \times R$ value, with the help of NMOS switches. This is depicted in Figure (6).

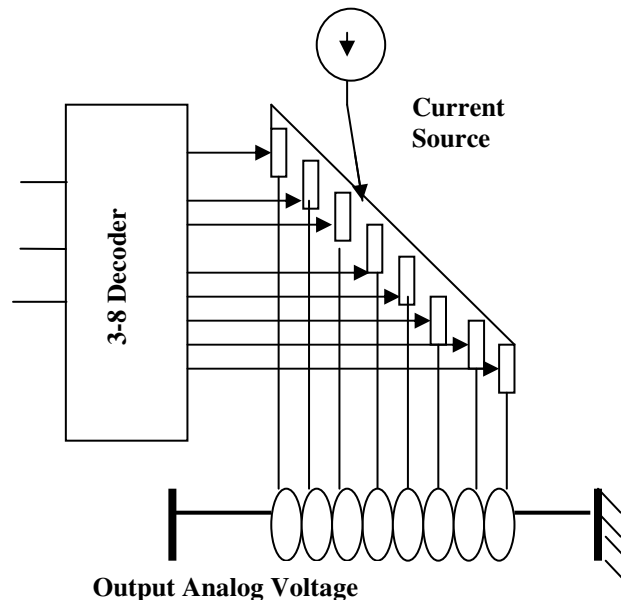


FIGURE 6: DAC using 8 NMOS switches at spring tap

Input							Output		
I_6	I_5	I_4	I_3	I_2	I_1	I_0	O_2	O_1	O_0
0	0	0	0	0	0	0	0	0	0
0	0	0	0	0	0	1	0	0	1
0	0	0	0	0	1	1	0	1	0
0	0	0	0	1	1	1	0	1	1
0	0	0	1	1	1	1	1	0	0
0	0	1	1	1	1	1	1	0	1
0	1	1	1	1	1	1	1	1	0
1	1	1	1	1	1	1	1	1	1

Table 1: 7-to-3 Priority Encoder

5. ELECTROMAGNETIC AD/DA CONVERTERS

In the case of electromagnetic field AD/DA converters the same arrangements of tapping positions are used here. Their positions and the coil geometrical dimensions, thought, need to be calculated for proper functioning.

In the case of ADC, only one coil of a certain dimension is used for the input analog voltage. The torque or deflection and hence tapping positions, are all linearly proportional to the input current, since both, the magnetic field and coil lengths are constant. Therefore tapping or contact positions are distributed linearly on the perimeter of the plate deflection path. It must be noted that this path should not extend beyond 90° deflection. As the deflection plate moves, logic high signals are inputted to the priority encoder, resulting; a binary digital output to be generated.

In the case of DAC, a number of coils, depending on the input bits, are embedded within the actuating plate. The dimensions [length X width] of these coils are proportional to their bits order. Since square windings are used, thus the torque is linearly proportional with the square of windings lengths, i.e. $T = kl^2$, where k is a constant. Figure (7) depicts the relation between torque and winding lengths and positions of the embedded winding coils.

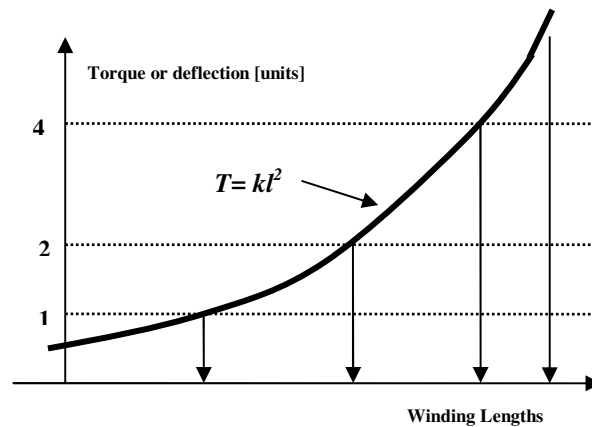


FIGURE 7: Electromagnetic DAC

6. CONCLUSION

It has been demonstrated that MEMS analog-to-digital and digital-to-analog converters can be formed using electrostatic and electromagnetic fields actuators. In the former, two plated capacitors with a damping spring arrangement is, whereas in the latter, coils embedded in a deflecting plate exposed to constant field, are employed.

MOS switches and contact positions of the converters are calculated according to the formulae governing the two fields. Whereas a certain input/output bits number is used, this arrangement can be expanded to a larger number.

7. REFERENCES

1. Chang Liu, "*Foundations of MEMS*", Prentice Hall, PP 105-321 (2006)
2. Sabih H. Gerez, "*Algorithms for VLSI Design Automation*", John Wiley, PP 41-131 (1999)
3. John Yeager, "*Low Level Measurements*", Keithley, 5th edition, PP 2.2 –3.25 (2000)
4. John. Craig, "Introduction to Robotics", Prentice Hall, PP 242-300 (2005)
5. W. Bolton, "*Mechatronics; Electronic Control Systems*", Prentice Hall, PP 24-47 (1999)

TCP Performance Measurement in GPRS Link Adaptation Process

Al-Khalid Othman

*Faculty of Engineering
Universiti Malaysia Sarawak
Kota Samarahan, 94300, Sarawak, Malaysia*

okhalid@feng.unimas.my

Muzalina Zakaria

*Faculty of Engineering
Universiti Malaysia Sarawak
Kota Samarahan, 94300, Sarawak, Malaysia*

muzalina_zakaria@yahoo.com

Khairuddin Ab. Hamid

*Chancellery
Universiti Malaysia Sarawak
Kota Samarahan, 94300, Sarawak, Malaysia*

khair@cans.unimas.my

Abstract

This paper presents the results of measured TCP performance in the LA process during the deployment of GPRS CS1 and CS2 coding schemes and after the activation of two more coding schemes, CS3 and CS4. The measurements are done under various network scenarios based on users' physical locations in one of Malaysia's commercially deployed live GPRS networks. End-to-end FTP file transfer application is used for the assessment together with tracing at the GPRS air interface. The results show that TCP works well in the LA process and can adapt to the frequent switching between the coding schemes without any problem. The average throughput is increased by 23% for urban areas owing to the activation of higher coding schemes and aided by TCP tuning. It is also shown that bad radio condition is the main factor affecting throughput. TCP performance is seen to be constant in all scenarios and it can cope with GPRS mobility and bad radio condition, although at the expense of reduced throughput.

Keywords: GPRS, TCP, Performance, Link Adaptation, Coding Scheme, Network Scenarios.

1. INTRODUCTION

General Packet Radio Service (GPRS) [1], [2] is an extension of Global System for Mobile communications (GSM) network. It offers packet-switched data transmission over the GSM air interface with efficient radio protocols to cover for erroneous data packets. GPRS provides 'always connected, always online' data services such as Internet applications to mobile users with data rate between 36.2kbps to 85.6kbps for four time slots allocation.

Internet applications such as web surfing, e-mail and file transfer rely on Transmission Control Protocol (TCP) [3] as a reliable transport for data transfers. It is a connection-oriented, packet-

switched transport method that delivers data in small segments or packets. TCP ensures ordered, error-free data delivery with its sequence numbering and acknowledgment systems together with retransmission of loss packets and checksum evaluation. Additionally, it provides data flow control through its congestion control mechanisms.

TCP is originally designed for data transfers across wired, fixed networks [4]. It anticipates transmission problems that are typical with wired networks behaviors. With the implementation of GPRS, TCP traverses the wireless mobile network which is a different environment from the wired network. The varying radio conditions expose data transfers over the wireless GPRS network to transmission errors. Accordingly, four GPRS coding schemes, CS1 to CS4, are defined and employed to protect data from these errors [5]. Switching between the coding schemes is dynamically done through a process called link adaptation (LA) [6]. The LA process may cause some impacts on the performance of Internet applications over live GPRS network. Moreover, due to the mobility factor, GPRS users are subjected to several network scenarios based on their physical locations. For example in urban areas, common locations for GPRS users are inside buildings, or outdoors in moving vehicles. The performance of Internet applications as perceived by users may vary depending on these scenarios. These issues have not been specifically addressed in the previous studies conducted on TCP performance in GPRS network [7], [8], [9].

There is a necessity to conduct measurements at the TCP layer to see the effects of the LA process on TCP performance. What are the TCP behaviors in different coding schemes? What are the factors that affect TCP performance? Are higher coding schemes giving a better TCP performance? Is it really beneficial and worthwhile to upgrade the coding schemes? Furthermore, all these are to be observed in a live network where there are many other factors beyond control like time slots availability, signal quality, users' mobility, and test environments that will give impact to the overall TCP performance, directly or indirectly. Therefore, to have more conclusive results, TCP performance measurement in GPRS LA process under different network scenarios ought to be taken under consideration.

This paper evaluates and compares the TCP performance throughout the LA process in one of the commercially deployed GPRS networks based on the initial coding schemes employment CS1 and CS2, and after the activation of higher coding schemes, CS3 and CS4. This is accomplished by incorporating TCP packet captures in GPRS drive-test measurements carried out in different scenarios based on GPRS users' typical locations in urban environment. TCP tuning is done as well to optimize the performance.

The TCP throughput and the TCP behaviors observed are examined together with GPRS tracing at the air interface. It is shown that TCP can adapt well to the LA process without any problem. The throughput improvement is moderate at best and is mainly governed by the current coding scheme used. TCP is seen to be affected by long delays encountered during data transfers that trigger its slow start process and further reduce the already low throughput achieved. The results obtained are only relevant to the particular GPRS network being assessed, thus may not apply to all GPRS networks in general.

The rest of the paper is organized as follows: section 2 outlines briefly the GPRS LA process together with GPRS parameters setup as implemented in this commercial network. Section 3 describes network scenarios selected for the measurements. Section 4 gives the overview of the TCP tuning done. In section 5, measurement set up is presented. The results obtained are discussed in Section 6. Finally, the conclusions of the study are given in Section 7.

2. GPRS LA PROCESS AND PARAMETERS SETUP

Table 1 gives the GPRS coding scheme with the associated throughput per time slot. In bad channel condition with high anticipated transmission errors, a stringent coding scheme is used

that will give the highest protection to the data during transfer but at the expense of reduced throughput. Higher coding schemes offer less protections and are applied during better channel conditions, thus yielding higher throughput [10].

Coding Scheme	Throughput (kbps)
CS1	9.05
CS2	13.4
CS3	15.6
CS4	21.4

TABLE 1: GPRS Coding Scheme and Associated Throughput.

The radio quality determines the appropriate coding scheme to be utilized. Since radio quality fluctuates over time, the coding schemes also keep on changing according to the varying conditions. In live network, the LA process or the switching between these different coding schemes is done dynamically by the network.

Table 2 provides the main GPRS Reliability class 3 [11] parameters setting for the network under evaluation in two separate measurements, Measurement 1 (M1) and Measurement 2 (M2). Since measurements are done in a live network, there is no control over some of the GPRS parameters that are changed according to the network conditions at the time. These include the LA process and time slot allocations. Four downlink time slots are allocated for GPRS but at anytime especially during congested or peak hours, they can be assigned to voice traffic which is given the priority over data. For this network, frequency hopping is not enabled.

Measurement 1 (M1)	
GPRS Network Parameter	Setting
LLC Mode	Unacknowledged
RLC Mode	Acknowledged
Downlink Timeslot Allocation	4
Channel Coding	CS1, CS2
Measurement 2 (M2)	
GPRS Network Parameter	Setting
LLC Mode	Unacknowledged
RLC Mode	Acknowledged
Downlink Timeslot Allocation	4
Channel Coding	CS1, CS2, CS3, CS4

TABLE 2: GPRS Parameters Setting.

Tracing at the air interface will keep track on time slot allocation and coding scheme usage together with the mobile's operating modes.

3. NETWORK SCENARIOS

Four common network scenarios associated with GPRS users' typical locations in urban areas are identified for the TCP performance measurements. The scenarios are outdoor stationary, outdoor moving, indoor stationary and indoor moving.

For outdoor stationary, the sites are chosen based on the highest GPRS usage rate and at the least congested GSM cell to avoid contention between voice and data traffic. These include the city centers, business districts, industrial areas and residential areas. The exact locations are picked to be near the serving cells as much as possible in order to have the best coverage. The

measurements are done by stopping outside buildings, at the open sidewalks and by the roadsides.

For outdoor moving, the measurements are carried out by driving along the identified drive route that covers areas with high GPRS usage, mainly the city centers and business neighborhoods. The driving speed is between 40 – 60km/h and is kept constant as much as possible.

For indoor stationary, buildings with indoor antenna are chosen such as shopping malls and hotels. Most of these have only one serving GSM cell. Residential buildings without the indoor antenna are also included. The measurements are carried out by sitting inside these buildings; the locations are deep or mid indoor and also indoor near the windows.

For indoor moving, the locations are the same as in indoor stationary scenario except that the measurement is carried out by walking in normal pace inside these buildings.

4. TCP TUNING

TCP operations depend greatly on the operating system at client's and server's ends. For this evaluation study, both client and server use Microsoft Windows XP Professional SP2 that supports modern TCP implementation with slow start, congestion avoidance, fast retransmit and fast recovery algorithms [12]. In addition, Selective Acknowledgement (SACK), window scaling and timestamp options are also supported.

To optimize TCP performance in the wireless GPRS network, TCP tuning is done at the client and/or the server ends according to the recommendations in RFC 3481 [13]. The main TCP parameters tuned with the associated values are presented in Table 3. These TCP parameters are adjusted to accommodate the low bandwidth, high delay GPRS network.

TCP Parameter	Value	Host	Remarks
Window Size	64kB	Client & Server	Based on Bandwidth Delay Product (BDP)
Path MTU Discovery	Enabled	Server	For Maximum Transmission Unit (MTU)
SACK	Enabled	Client & Server	Acknowledging non-contiguous packets
Timestamps	Enabled	Client & Server	More and better RTT samples

TABLE 3: Tuned TCP Parameters.

GPRS Bandwidth Delay Product (BDP) is around 1 – 5kB [13] hence the 64kB window size is sufficient and window scaling option is not required. To determine the TCP Maximum Segment Size (MSS), Path MTU Discovery option is enabled. SACK option is turned on to provide acknowledgments for non-contiguous or out-of-order data packets. This will prevent the sender from retransmitting successfully received packets which can affect the throughput. Timestamp option gives the benefit of obtaining more Round-Trip Time (RTT) samples including for the retransmitted data packets. By default, Windows XP Pro uses the initial send window of two segments size.

5. MEASUREMENT SETUP

As mentioned, two separate measurements are carried out, M1 and M2. M1 is done during the implementation of CS1 and CS2 only, and M2 is performed after the activation of CS3 and CS4. Both M1 and M2 are carried out at the same physical locations as much as possible in all scenarios.

For the measurements, File Transfer Protocol (FTP) application is used to assess the TCP performance. A 500kB file download is carried out from the server to the client as per Figure 1.

The bulk data download using FTP can give insights to TCP steady-state behaviors. Hence, only FTP data connection is considered to compute the performance metrics in the server-to-client direction that corresponds to GPRS downlink direction.

For each defined scenario, 32 to 60 repetitive file transfers are performed. At both server and client ends, Wireshark [14] is used to capture the TCP packets exchanged. The captures are then analyzed using tcptrace [15]. Concurrently, TEMS Investigation [16] is run at the client side to capture on GPRS air interface using a class 10 (4 Downlink + 2 Uplink) mobile phone. This supports four time slots for downlink data transfer.

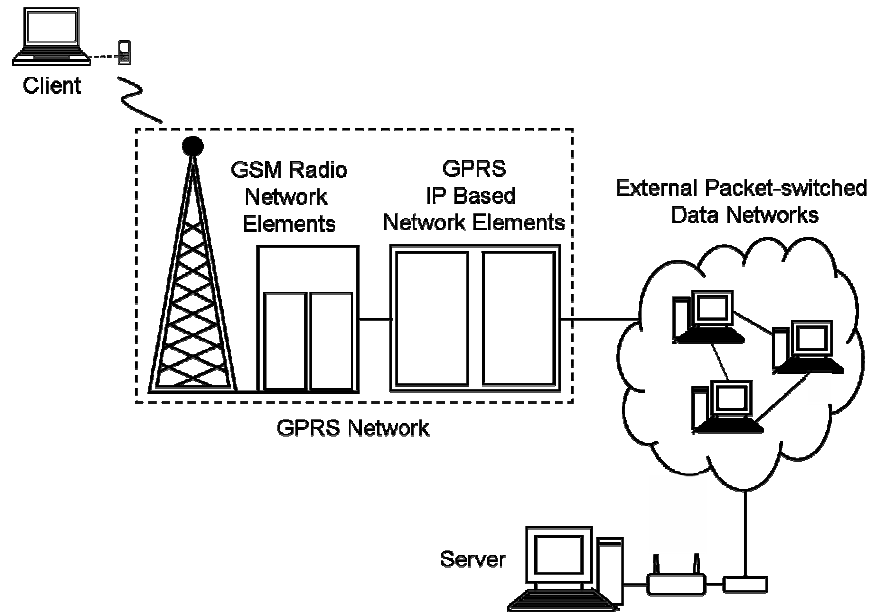


FIGURE 1: Measurement Setup.

6. MEASUREMENT RESULTS

6.1 TCP Throughput and Packet Loss

For both M1 and M2, the throughput results are described by the average, max (maximum) and min (minimum) of the total throughput for the whole data transfers in all scenarios and the total throughput for all data transfers in each scenario.

Figure 2 presents the comparison on the client's overall throughput obtained from both measurements. The highest CS data rate is according to CS2 and CS4 with four time slots allocations. The average throughput is computed based on transmitted data bytes over transfer time excluding headers.

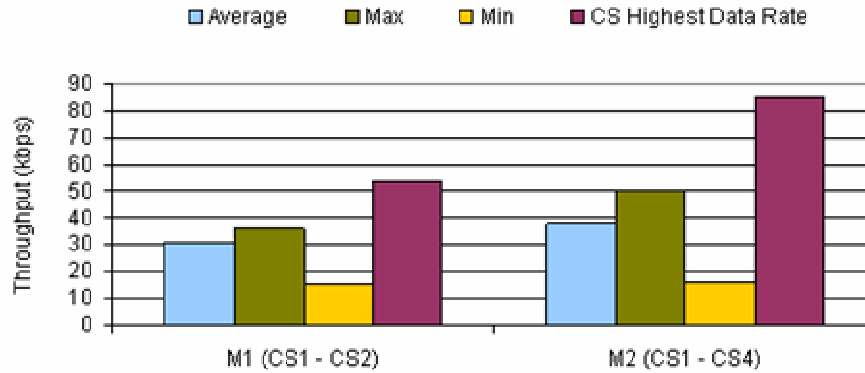


FIGURE 2: Client Downlink Overall Throughput.

M2 performs better than M1 in terms of average and max throughputs. The average throughput for M1 is 31kbps and for M2, the average throughput is 38kbps. The increase is approximately 23%, thus proving the benefit of activating higher coding schemes in improving the throughput [17]. This is further exemplified by the approximately 38% increment in the max throughput achievable i.e. from 36kbps for M1 to 50kbps for M2. Yet, the percentage ratio of the increase in average throughput to the increase in the highest available data rate is 23:60 which indicates that the available high data rate provided by the activation of CS3 and CS4 is still underutilized i.e. less than 50%. Both measurements obtain similar minimum throughput which is around 15 – 16kbps since both have the same lower coding scheme limit.

Figure 3 splits the overall throughput into throughput based on different network scenarios. For M1, the average throughput is seen to be almost constant for each scenario, ranging between 26kbps to 33kbps. For M2, the average throughput is between 33kbps to 42kbps and also almost constant for all scenarios. These lead to an almost uniform average throughput increment for each scenario; 20% in outdoor stationary, 28% in outdoor moving and indoor stationary and 21% in indoor moving. The maximum throughput achieved for M1 is around 60 – 67% of CS2 data rate and also constant for all conditions. Mobility factor has an influence on the minimum throughput which is about 15 – 28kbps. The minimum throughput is noted to be lower while on the move compares to during stationary condition. The maximum achievable throughput for M2 is between 40kbps to 50kbps. All scenarios in M2 give more or less the same minimum throughput as M1 except outdoor moving. In this scenario, the minimum throughput is 27kbps for M2 compares to only 16kbps in M1.

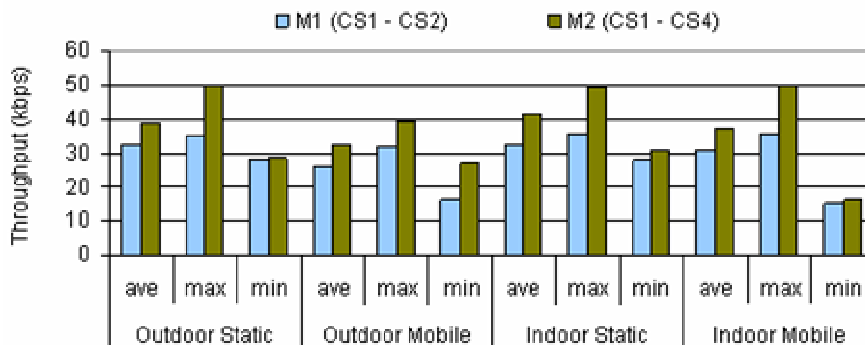


FIGURE 3: Client Downlink Throughput Based On Network Scenarios.

It is evident from the constant throughput performance observed in each scenario for both measurements that the network is consistently experiencing bad radio conditions. In M1, average throughput per time slot is around 6.5kbps to 8.25kbps and in M2, it is between 8.25kbps to 10.5kbps. These correspond to CS1 data rate, indicating the worst channel condition. Mobility gives some impact on lowering the average throughput further since it is predisposed to cell reselection and temporary absence of radio resources on top of the bad radio conditions experienced.

In M1, the LA process involves switching between two coding schemes; while in M2, it involves four coding schemes, thus introducing variable throughput maximized for different radio conditions [18]. Therefore, for M1, the throughput variation may not be great from one scenario to another since the option is either CS1 for bad condition and CS2 for slightly better or good conditions. It is expected that for M2, besides an overall throughput increment from M1 provided by the CS3 and CS4 higher data rates, a wider range of throughput should be seen for different scenarios. However, the fact that both measurements have constant low average throughput in the range of CS1 data rate points to a degraded radio condition experienced in all scenarios for most of the time during data transfers. Max throughput obtained from both measurements further substantiates this fact. It will be shown that CS1 is the dominant coding scheme used during data transfers for both M1 and M2.

From the client's traces, low throughput is also contributed by periods of idle time when almost no flow of data happens. The GPRS traces in Figure 4 (a) reveal that the idle times are the result of the mobile's idle mode and cell reselection which are seen in all scenarios. These are the sources of long sudden delays during data transfers [19]. During these moments, radio resources become temporarily unavailable. Data transmission process is suspended for some time while waiting for the radio resources to be available again as seen in Figure 4 (b) for the TCP time sequence graph. If this last long enough until TCP timeout timer expires, TCP will go into its slow start mechanism since it assumes congestion has taken place [20]. TCP requires extra time to recover from this temporary outage and to get the data flow back to normal. As depicted in Figure 4 (d), the slow start process after the temporary outage takes approximately 5s. This contributes to the wastage of radio resources and lengthens the data transfer time, thus reducing throughput.

Frequent switching between the coding schemes especially in M2 does not affect TCP by way of disrupting or suspending data transfers as observed in Figure 4 (a) – (c). TCP throughput is fluctuating as observed in Figure 4 (c) for the TCP throughput graph, following the switching of the coding schemes. TCP is shown to adapt very well to the LA process without any problems.

TCP handles data packet loss by retransmission mechanism. During mobile idle mode or a cell reselection, very few packets are lost, normally between one to five packets. However, if these occur in succession, the total of lost packets would be substantial. This is shown in Figure 5 (a) and 5 (c). Prolonged bad channel condition is another reason for retransmissions as seen in Figure 5(b) and 5(d). Packet loss reduces throughput in a way that it lengthens the transfer time due to packet retransmissions.

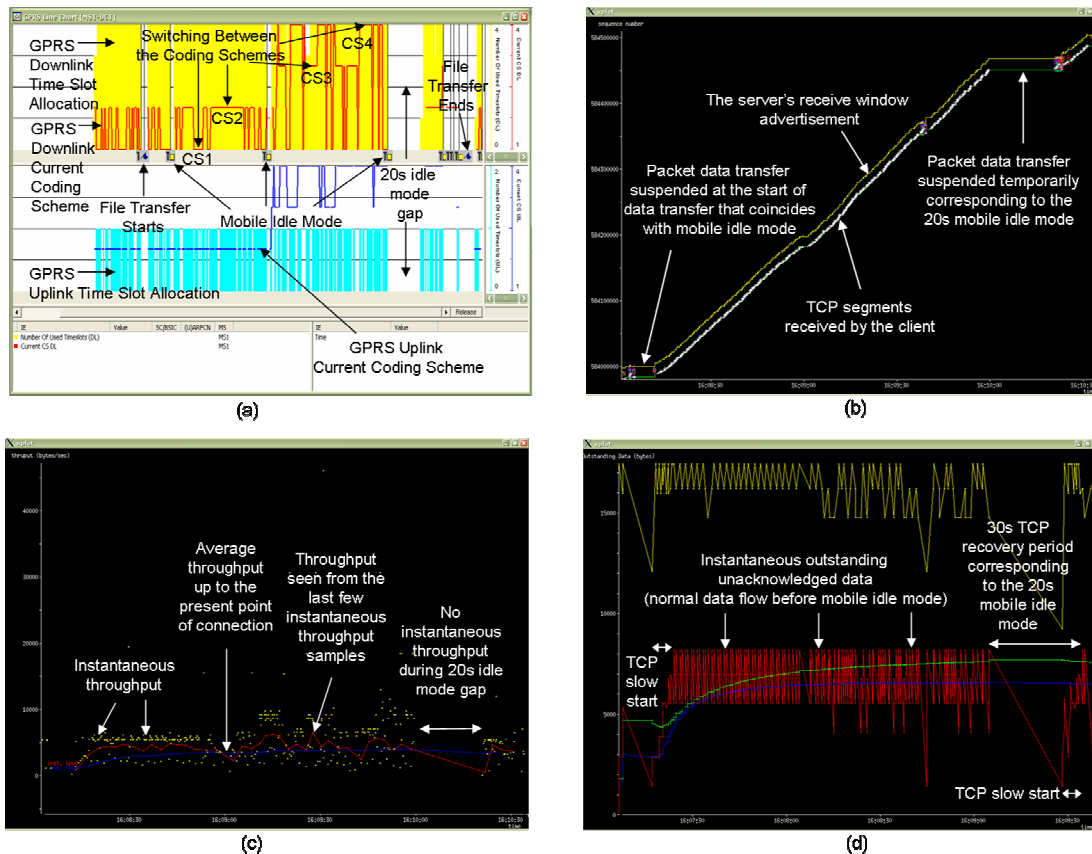


Figure 4: Low Throughput Due To Mobile Idle Mode. Clockwise – (a) LA Process and Mobile Idle Mode. (b) Suspension of Data Transfer During Mobile Idle Mode. (c) Zero Throughput During Mobile Idle Mode. (d) TCP Recovery Period.

6.2 GPRS Traces

Figure 6 represents the overall current coding scheme usage and time slot allocations for M1 and M2. It is shown that in both measurements, CS1 dominates half of the coding scheme usage during transfer time. Bad radio condition is the main contributing factor for the constant low average throughput obtained for each scenario in M1 and M2. This affects the overall average throughput that manages only to reach more or less 50% of the highest available data rate with four time slots allocation. Some studies for example in [8], emphasize more on TCP mechanisms interacting badly with GPRS resources which in turn, causes low throughput. Yet, from the findings, the prevalent factor is the bad radio condition represented by the CS1 scheme. The TCP mechanisms are only an additional factor on top of the bad radio condition.

Combined with packet loss and lengthy TCP recovery periods during mobile idle mode, throughput is further compromised. Coding scheme depends on current radio condition and good radio condition is therefore crucial to ensure optimum data throughput.

Four dedicated time slots are allocated for GPRS downlink data transfer as per Figure 6. However, this allocation is dynamically changed according to voice traffic congestion. The availability of four time slots for most of the data transfers shows that there is minimum contention with voice traffic and ensures throughput is not further affected. Hence, voice traffic congestion is not a particular concern for this network.

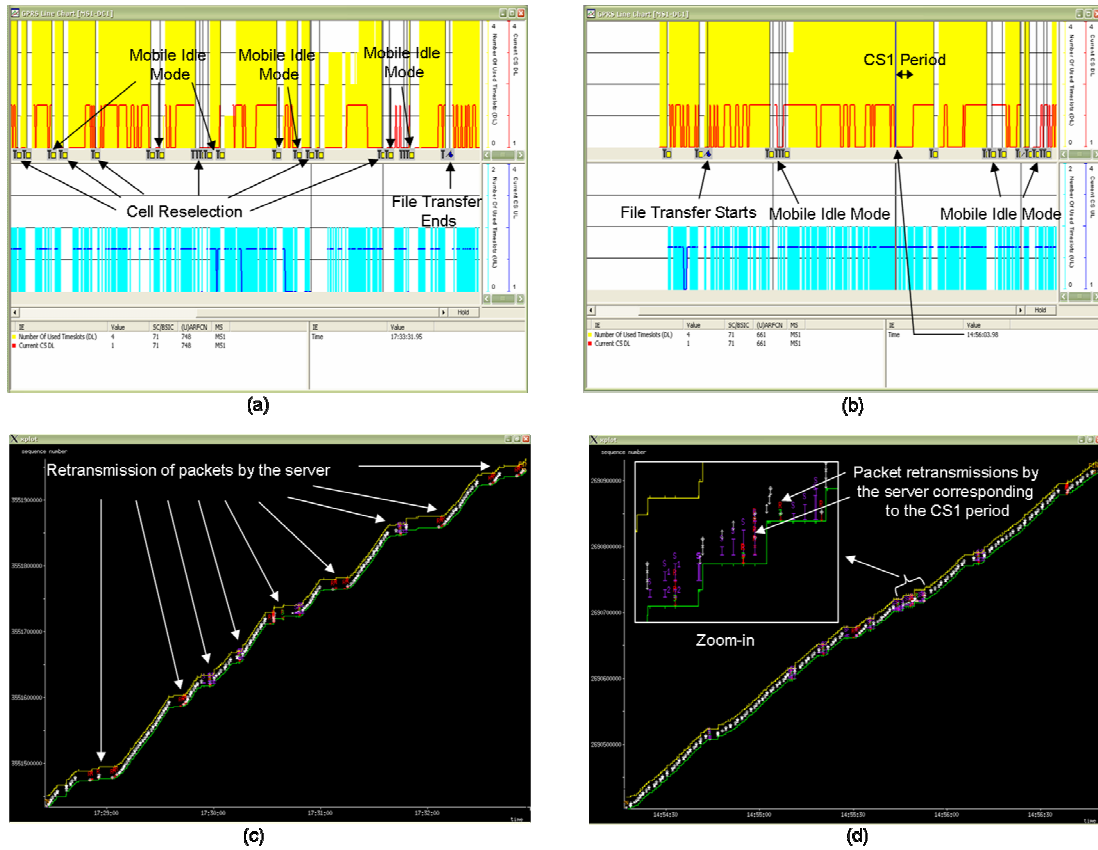


Figure 5: Packet Loss Due to Mobile Idle Mode or Cell Reselection. Clockwise – (a) Successive Mobile Idle Mode and Cell Reselections. (b) Prolonged Bad Channel Condition. (c) Successive Retransmissions (R). (d) Retransmissions (R) During CS1 Period.

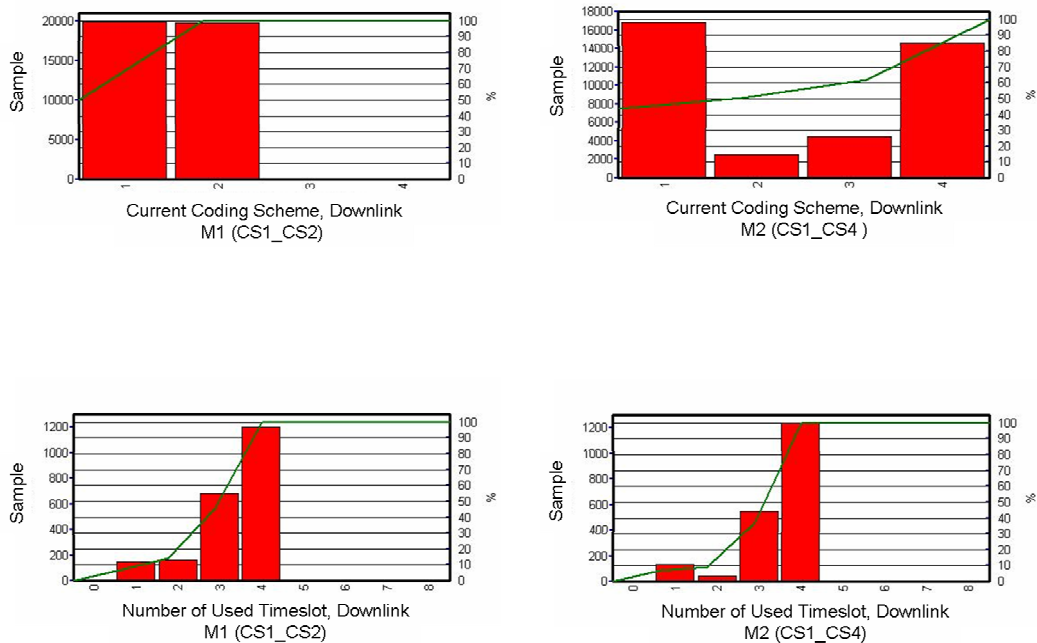


Figure 6: Overall Downlink Current Coding Scheme Usage and Time Slot Allocations.

7. CONCLUSIONS

TCP adapts well in the LA process and can cope with the frequent switching between the coding schemes without any problem. The activation of higher coding schemes does not increase TCP performance much because of the consistently bad radio conditions experienced during data transfers for all scenarios. Unless radio condition is improved, the benefit of activating higher coding schemes will not be apparent. To fully utilize the high data rates provided by CS3 and CS4 coding scheme, the network operator must ensure good radio conditions in all scenarios.

TCP performance is degraded more during mobility in GPRS because of predisposition to long delays. It is observed to be affected by temporary absence of radio resources during mobile idle mode, cell reselections and rarely, persistent bad channel conditions where packet loss is common. This triggers TCP into slow start and congestion avoidance modes thus affecting throughput.

8. REFERENCES

1. C. Bettstetter, H. J. Vögel and J. Eberspacher. "GSM Phase 2+ General Packet Radio Service GPRS: Architecture, protocols and air interface". IEEE Communications Surveys, 2(3):2-14, 1999
2. G. Brasche and B. Walke. "Concepts, services and protocols of the new GSM Phase 2+ General Packet Radio Service". IEEE Communications Magazine, 35(8):94-104, 1997
3. W. R. Stevens. "TCP/IP Illustrated, Volume I: The Protocols", Addison Wesley, (1994)
4. Information Sciences Institute, University of Southern California. "Transmission Control Protocol". RFC793, 1981
5. 3GPP TS 45.003. "Radio Access Network; Channel coding". Release 7, 2007
6. E. Seurre, P. Savelli and P-J Pietri. "GPRS for Mobile Internet", Artech House, (2003)
7. M. Meyer. "TCP performance over GPRS". Wireless Communications and Networking Conference, 1999, 3:1248-1252, 1999
8. R. Chakravorty, J. Cartwright, and I. Pratt. "Practical experience with TCP over GPRS". Global Telecommunications Conference, 2002, 2(17-21):1678-1682, 2002
9. J. Korhonen, O. Aalto, A. Gurtov and H. Lamanen. "Measured performance of GSM HSCSD and GPRS". IEEE International Conference on Communications, 2001, 5:1330-1334, 2001
10. 3GPP TS 43.064. "General Packet Radio Service (GPRS); Overall description of the GPRS radio interface; Stage 2". Release 7, 2007
11. 3GPP TS 03.60. "Digital cellular telecommunications system (Phase 2+); General Packet Radio Service (GPRS); Service description; Stage 2". Release 1998, 2002
12. <http://www.microsoft.com>, Microsoft Windows XP Professional Product Documentation – TCP/IP RFCs
13. H. Inamura, G. Montenegro, R. Ludwig, A. Gurtov and F. Khafizov. "TCP over Second (2.5G) and Third (3G) Generation wireless networks". RFC3481, 2003
14. <http://www.wireshark.org>, Wireshark

A.K. Othman, M. Zakaria, K. Ab. Hamid

15. <http://www.tcptrace.org>, tcptrace
16. Ericsson. *"TEMS Investigation 7.1 Data Collection User's Manual"*, (2006)
17. W. Featherstone and D. Molkdar. *"Capacity benefits of GPRS coding schemes CS-3 and CS-4"*. IEE Conference Publication, (489):287-291, 2002
18. 3GPP TS 45.050. *"Radio Access Network; Background for Radio Frequency (RF) requirements"*. Release 7, 2007
19. A. Gurtov. *"Effect of delays on TCP performance"*. IFIP Conference Proceedings, Proceedings of the IFIP TC6/WG6.8 Working Conference on Emerging Personal Wireless Communications. 195:87-108, 2001
20. M. Allman, V. Paxson and W. Stevens. *"TCP congestion control"*, RFC 2581, 1999

Atmospheric Non-Thermal Plasma Sources

Vijay Nehra

*Deptt of Electronics & Communication
Guru Jambheshwar University of Science & Technology
Hisar-125001, India*

nehra_vijay@yahoo.com

Ashok Kumar

*YMCA Institute of Engineering & Technology
Faridabad-121006, India*

ashokarora123@yahoo.co.in

H K Dwivedi

*R & D Head (PDP)
Samtel Color Limited
Ghaziabad-201001, UP, India*

harish1147@gmail.com

Abstract

Atmospheric non-thermal plasmas (ANTPs) have received a great deal of attention in the last two decades because of their substantial breakthrough in diverse scientific areas and today technologies based on ANTP are witnessing an unprecedented growth in the scientific arena due to their ever-escalating industrial applications in several state-of-the-art industrial fields. ANTps are generated by a diversity of electrical discharges such as corona discharges, dielectric barrier discharges (DBD), atmospheric pressure plasma jet (APPJ) and micro hollow cathode discharges (MHCD), all having their own characteristic properties and applications. This paper deals with some fundamental aspects of gas discharge plasmas (GDP) and provides an overview of the various sources of ANTps with an emphasis on dielectric barrier discharge.

Keywords: Atmospheric plasma, Non-thermal, Dielectric barrier discharge.

1. INTRODUCTION

Since the past two decades, considerable efforts have been made by the scientific and technological community to generate, sustain and utilize ANTP because of their numerous scientific and industrial applications. Growth and importance of atmospheric cold plasma technology can be realized by the fact that the scientific and technological utilization of ANTP has multiplied by several factors and its applications have expanded into a large number of fields such as in environmental engineering, aeronautics and aerospace engineering, biomedical field, textile technology, analytical chemistry, and several other areas too. The enormous promise of atmospheric non-thermal technology stems from its remarkable potential for being environment friendly & energy-saving, its flexibility & capability for creation of new products and its clear ecological advantages. Unique features, diversified applications and a vast array of opportunities offered in a large number of diverse and unrelated fields has made it indispensable enough to harness their potential in the scientific and industrial areas. Keeping in view the huge potential of GDPs in several diversified fields, this article serves to

provide an overview of atmospheric non-thermal plasma. Most of the earlier studies on man-made plasmas were focused at low pressure, but the last two decades have witnessed a growing attention to generate GDP at elevated pressure, preferably close to atmospheric pressure. This is a challenging task due to instabilities of glow to arc transitions. At present, several approaches are being used to produce ANTP, out of which a few common approaches have been briefly discussed in this paper [1-11].

The paper is mainly divided into two parts. For a better understanding of the phenomena of GDP, one should have an acquaintance of the various parameters that one has to deal with in the gas discharges. Some of these fundamental aspects of GDP are discussed in the first half of the paper. The succeeding section mainly focuses on commonly used ANTP schemes such as corona, APPJ, MHCD, and DBD.

2. FUNDAMENTAL ASPECTS OF GDP

2.1 Plasma: Introduction

Plasma, a quasi-neutral gas, is considered to be the fourth state of matter, following the more familiar states of solid, liquid & gas and constitutes more than 99% matter of the universe. It is more or less an electrified gas with a chemically reactive media that consists of a large number of different species such as electrons, positive and negative ions, free radicals, gas atoms and molecules in the ground or any higher state of any form of excited species (fig. 1). It can exist over an extremely wide range of temperature and pressure. It can be produced at low-pressure or atmospheric pressure by coupling energy to a gaseous medium by several means such as mechanical, thermal, chemical, radiant, nuclear, or by applying a voltage, or by injecting electromagnetic waves and also by a combination of these to dissociate the gaseous component molecules into a collection of ions, electrons, charge-neutral gas molecules, and other species. It is thus an energetic chemical environment that combines particles and radiations of a diverse nature, an incredibly diverse source of chemistry that is normally not available in other states of matter. Parallel to the generation of plasma species, loss processes also take place in the plasma. In fact, all energy ends up as heat with a small fraction invested in surface chemistry.

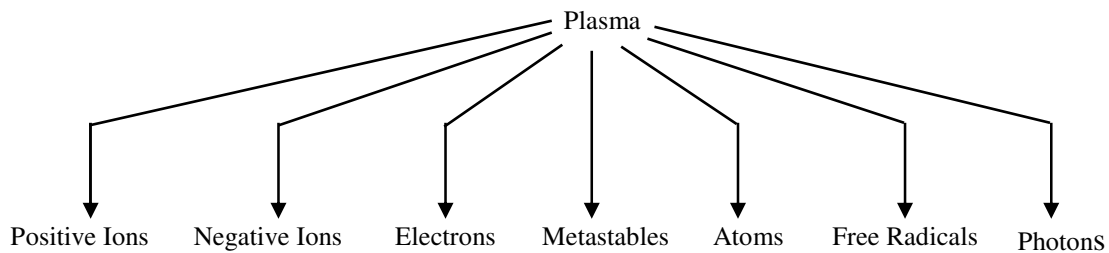


Figure 1: Constituents of plasma

2.2 Classification of plasma

Broadly speaking, plasmas can be distinguished into two main groups *i.e.*, the high temperature or fusion plasmas and the so called low temperatures or gas discharges. A typical classification and parameters of different kinds of plasmas is given in table 1. High temperature plasma implies that all species (electrons, ions and neutral species) are in a thermal equilibrium state. Low temperature plasma is further subdivided into thermal plasma, also called quasi-equilibrium plasma, which is in a local thermal equilibrium (LTE) state, and non thermal plasma (NTP), also called nonequilibrium plasma or cold plasma.

Plasma	State	Example
High temperature plasma (Equilibrium plasma)	$T_e \approx T_i \approx T_g, T_p = 10^6 - 10^8 K$ $n_e \geq 10^{20} m^{-3}$	Laser fusion plasma
Low temperature plasma		
Thermal plasma (Quasi-equilibrium plasma)	$T_e \approx T_i \approx T_g \leq 2 \times 10^4 K$ $n_e \geq 10^{20} m^{-3}$	Arc plasma, plasma torches, RF inductively coupled discharges
Non thermal plasma (Non-equilibrium plasma)	$T_e \gg T_i \approx T_g = 300 \dots \dots \dots 10^3 K$ $n_e \approx 10^{10} m^{-3}$	Glow, corona, APPJ, DBD, MHCD, OAUGDP, plasma needle etc

Table1: Classification of plasma

Thermal plasmas (TP) are characterized by an equilibrium or near equality between electrons, ions and neutrals. Commonly employed thermal plasma [12-20] generating devices are those produced by plasma torches, and microwave devices. These sources produce a high flux of heat and are mainly used in areas such as in plasma material processing and plasma treatment of waste materials. High temperature of TPs can process even the most recalcitrant wastes including municipal solids, toxic, medical, biohazard, industrial and nuclear waste into elemental form, ultimately reducing environmental pollution caused due to them. But for several technological applications, the high temperature characteristic of TPs is neither required nor desired, and in some cases it even becomes prohibitive. In such application areas, cold plasmas become more suited.

Cold plasmas refer to the plasmas where most of the coupled electrical energy is primarily channeled to the electron component of the plasma, thereby producing energetic electrons instead of heating the entire gas stream; while the plasma ions and neutral components remain at or near room temperature. Because the ions and the neutrals remain relatively cold, this characteristic provides the possibility of using cold plasmas for low temperature plasma chemistry and for the treatment of heat sensitive materials including polymers and biological tissues. The remarkable characteristic features of cold plasma that include a strong thermodynamic non-equilibrium nature, low gas temperature, presence of reactive chemical species and high selectivity offer a tremendous potential to utilize these cold plasma sources in a wide range of applications.

2.3 Plasma chemistry and origin of species

The chemistry [10, 21-22] which takes place in a plasma is usually quite complex and involves a large number of elementary reactions. The main types of reactions occurring in volume plasma are divided into homogenous and heterogenous reactions. Homogenous reactions occur between species in the gaseous phase as a result of inelastic collisions between electrons and heavy species or collisions between heavy species; whereas, heterogenous reactions occur between the plasma species and the solid surface immersed or in contact with the plasma. These typical reactions have been listed in table 2 (a) and (b). The heterogenous reactions are particularly important in the processing of semiconductor materials.

Name	Reactions	Description
Excitation of atoms or molecules	$e + A_2 \rightarrow A_2^* + e$ $e + A \rightarrow A^* + e$	Leads to electronically excited state of atoms and molecules by energetic electron impact.

De-excitation	$e + A_2^* \rightarrow A_2 + e + h\nu$	Electronically excited state emits electromagnetic radiations on returning to the ground state.
Ionization	$e + A_2 \rightarrow A_2^+ + e$	Energetic electrons ionize neutral species through electron detachment and positively charged particles are formed.
Dissociation	$e + A_2 \rightarrow 2A + e$	Inelastic electron impact with a molecule causes its dissociation without ions.
Dissociative attachment	$e + A_2 \rightarrow A^+ + A + e$	Negative ions are formed when free electrons attach themselves to neutral species.
Dissociative ionization	$e + A_2 \rightarrow A + e$	Negative ions can also be produced by dissociative ionization reactions.
Volume recombination	$e + A + B \rightarrow A + B$	Loss of charged particles from the plasma by recombination of opposite charges.
Penning dissociation	$M^* + A_2 \rightarrow 2A + M$	Collision of energetic metastable species with neutral leads to ionization or dissociation.
Penning ionization	$M^* + A \rightarrow A^+ + M + e$	
Charge exchange	$A^+ + B \rightarrow B^+ + A$	Transfer of charge from incident ion to the target neutral between two identical or dissimilar partners.
Recombination of ions	$A^- + B^+ \rightarrow AB$	Two colliding ions recombine to form a molecule.
Electron-Ion recombination	$e + A_2^+ + M \rightarrow A_2 + M$	Charge particles are lost from the plasma by recombination of opposite charges.
Ion-ion recombination	$A^+ + B^- + M \rightarrow AB + M$	Ion-ion recombination can take place through three body collisions.

Table 2 (a): Gas phase reactions involving electrons and heavy species

Name	Reactions	Description
Etching	$AB + C_{solid} \rightarrow A + BC_{vapour}$	Material erosion.
Adsorption	$M_g + S \rightarrow M_s$ $R_g + S \rightarrow R_s$	Molecules or radicals from a plasma come in contact with a surface exposed to the plasma and are adsorbed on surfaces.
Deposition	$AB \rightarrow A + B_{solid}$	Thin film formation.
Recombination	$S - A + A \rightarrow S + A_2$ $S - R + R_1 \rightarrow S + M$	Atoms or radicals from the plasma can react with the species already adsorbed on the surface to combine and form a compound.
Metastable de-excitation	$S + A^* \rightarrow A$	Excited species on collision with a solid surface return to the ground state.

Sputtering	$S - B + A^+ \rightarrow S^+ + B + A$	Positive ions accelerated from the plasma towards the surface with sufficient energy can remove an atom from the surface.
Polymerization	$R_g + R_s \rightarrow P_s$ $M_g + R_s \rightarrow P_s$	Radicals in the plasma can react with radicals adsorbed on the surface and form polymers.

Table 2 (b): Surface reactions

2. 4 Electrical breakdown of gases

2.4.1 Conditions for self sustained discharge

To sustain plasma, the applied voltage must exceed the breakdown voltage for the gases. When this voltage is reached, the gases lose their dielectric properties and turn into a conductor. The criteria for self sustaining is given as

$$1 - \gamma(e^{\alpha d} - 1) = 0$$

$$e^{\alpha d} = \left(1 + \frac{1}{\gamma}\right)$$

2.4.2 Paschen breakdown criteria

The breakdown voltage in gas discharge plasma is given as

$$V_b = \frac{Bpd}{\{\ln(Apd) - \ln[\ln(1 + \frac{1}{\gamma})]\}} \tag{1}$$

$V_b = f(pd)$, which is the Paschen law.

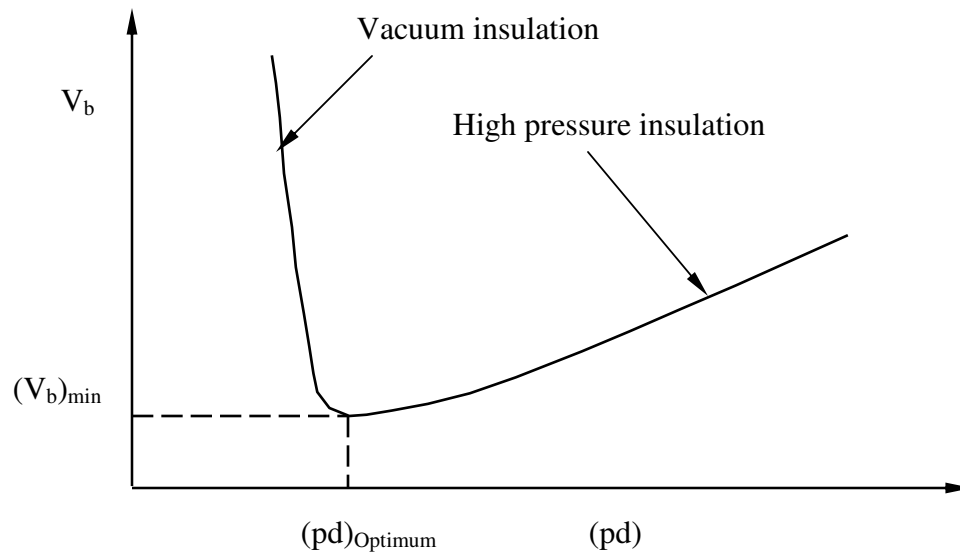


Figure 2: Paschen curve for breakdown voltage versus pd

From (1) it is obvious that breakdown voltage depends only on the product pd for a given gas and the cathode material, regardless of the individual values of p and d . The Paschen curves (fig. 2)

for different gases have roughly the same shape but are shifted from one another. From the curve, it is clear that there is a minimum breakdown voltage at a certain pd product and the breakdown potential is large for both small and large values of pd. At low pd values, the breakdown voltage is high because of too few collisions and at high pd values; the breakdown voltage is high because of too many collisions. The physical significance of this minimum voltage is that no matter how small the gap or pressure, it is impossible to strike a discharge at a voltage less than the minimum breakdown voltage [22-23].

3. ATMOSPHERIC NON-THERMAL PLASMA SCHEMES

Low pressure glow discharge plasmas are of great interest in fundamental research as well as in the microelectronic industry and material technology. But, these plasmas must be contained in costly air tight enclosures (massive vacuum reactors) making them highly expensive and time consuming. Also, the density of activated particles is relatively low. Therefore, one of the recent trends focuses on developing new plasma sources, which operate at atmospheric pressure, but retain the properties of low pressure media. The economic and operational advantages of operating at 1 atm have led to the development of a variety of atmospheric plasma sources for several scientific and industrial applications.

Thus, in the last two decades, ANTPs have attracted more attention due to their significant industrial advantages over low-pressure discharge. Non-thermal atmospheric plasma may be obtained by a diversity of electrical discharges such as corona discharge, micro hollow cathode discharge, atmospheric pressure plasma jet, gliding arc discharge, one atmospheric uniform glow discharge, dielectric barrier discharge, and plasma needle, all having important technological applications. The characteristic of all these atmospheric plasma sources in terms of plasma properties is shown in table 3. A brief description of commonly used forms of ANTP is illustrated in the succeeding sections.

Parameters	Corona Discharge	DBD	APPJ	Atmospheric glow MHCD
Method and Type	Sharply pointed electrode	Dielectric barrier cover on electrodes	RF capacitively coupled	DC glow with micro hollow cathode electrode
Excitation	Pulsed DC	AC or RF	RF 13.5 MHz	DC
Pressure (bar)	1bar	1bar	760 torr	1bar
Electron energies (eV)	5 variable	1-10	1-2
Electron Density, cm⁻³	10 ⁹ -10 ¹³ variable	≈10 ¹² -10 ¹⁵	10 ¹¹ -10 ¹²	
Breakdown Voltage (kV)	10-50	5-25	0.05-0.2
Scalability & Flexibility	No	Yes	Yes	Yes
T_{max} Temp T (K)	Room	Average gas Temp (300)	400	2000
Gas	N ₂ + O ₂ + NO+ Rare gas/Rare gas halides	Helium, Argon	Rare gas/Rare gas halides

Table 3: Plasma properties of atmospheric discharge schemes

3.1 Corona discharge

The first scheme that was used to generate ANTP was corona discharge [1, 2, 24-26]. It exists in several forms, depending on the polarity of the field and the electrode geometrical configuration. This type of discharge is the characteristic of an asymmetric electrode pair and results from the electric field that surrounds inhomogeneous electrode arrangements powered with a continuous or pulsed dc voltage. In a highly non-uniform electric field, as for example, point plane gap or wire cylindrical gap, the high electric field near the point electrode or wire electrode far exceeds the breakdown strength of the gas and a weakly ionized plasma is created. Coronas are thus inherently non-uniform discharges that develop in the high field region near the sharp electrode spreading out towards the planar electrode. This phenomenon of local breakdown is called corona discharge. Fig. 3 shows a schematic of point to plane corona. It is a positive corona when the electrode with the strongest curvature is connected to the positive output of power supply and a negative corona when this electrode is connected to the negative terminal of power supply. The development of a corona discharge progresses sequentially through the following steps: (1) an asymmetric electrode configuration is made; (2) a high voltage is applied, and some free electric charge is made available; (3) an avalanche builds up and leaves behind a space charge area; (4) photons from the avalanche create new charge carriers outside the space charge area; (5) a new avalanche develops closer to the cathode. The most important large-scale application of corona discharge is in electrostatic precipitators (ESP), which are used for dust collection in many industrial off gases. In addition to ESP, corona discharges are also used in water purification, electrophotography, copying machine, printers and liquid spray gun and in powder coating. However, the restricted area and the inherent non-uniformity have limited their application in material processing.

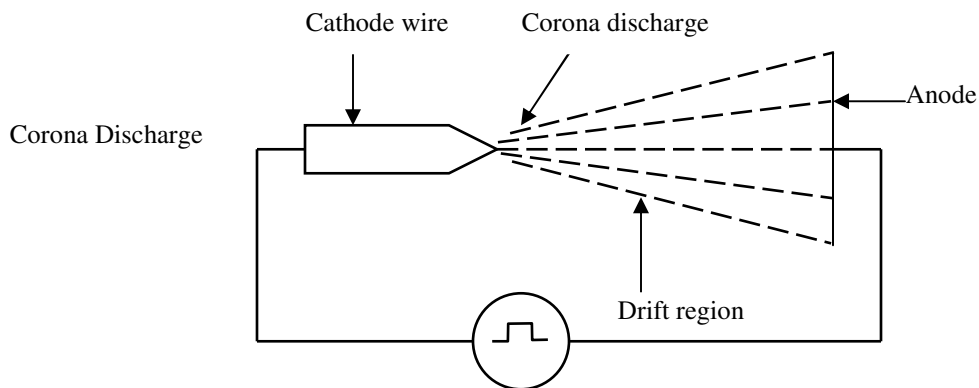


Figure 3: Schematic of corona discharge

3.2 Atmospheric-pressure plasma jet

Another kind of discharge capable of generating non-thermal plasmas at atmospheric pressure is atmospheric-pressure plasma jet. A schematic of the APPJ is shown in fig 4. The APPJ [27-32] developed by Jeong et al. (University of California, Los Angeles) in collaboration with Park et al. (Los Alamos National Laboratory) consists of two concentric electrodes through which a mixture of helium, oxygen or other gases flows. In this arrangement, the inner electrode is coupled to 13.56 MHz radio frequency power at a voltage between 100-250 V and the outer electrode is grounded. By applying RF power, the discharge is ignited and operates on a feed stock gas, which flows between an outer grounded, cylindrical electrode and a central electrode and produces a high velocity effluent stream of highly reactive chemical species. Central electrodes driven by radio frequency power accelerate free electrons. These energetic electrons undergo inelastic collisions with the feed gas, producing excited state molecules, atoms, free radicals and additional ion-electron pairs. Once the gas exits the discharge volume, ions and electrons are rapidly lost by recombination, but the fast flowing effluent still contains neutral metastable species and radicals. The key operational features of APPJ are as follows: (1) it produces a stable, homogeneous and uniform

discharge at atmospheric pressure; (2) operates at radio frequency (RF) power of 250 W and frequency of 13.56 MHz ; (3) the ionized gas from the plasma jet exits through the nozzle where it is directed onto the substrate and hence utilized in downstream processing; (4) it operates without a dielectric cover over the electrode, yet is free from filaments, streamers and arcing; (4) The gas temperature of the discharge is as low as 50°C, allowing it to treat delicate surfaces without damage, or as high as 300°C, allowing it to treat robust surfaces much more aggressively. (5) it exhibits a great similarity to low-pressure DC glow discharge. This technology shows promises for being used in material application that are now limited to vacuum. These features give APPJ the potential to be utilized in a large number of applications. It has major utilization in material processing, for example, applications ranging from etching polyamide, tungsten, tantalum and silicon dioxide as well as to deposit silicon dioxide film by plasma assisted chemical vapor deposition. The fast flowing effluent of reactive species in APPJ technology is also utilized in applications such as decontamination of materials having chemical and biological warfare agents and in the removal of radionuclide from surfaces and equipments. In addition, it is also used to clean large industrial parts more effectively than solvents; sterilization of surgical and dental equipments and hospital surfaces and removal of paint from brick, making it effective for graffiti removal; and in the textile industry.

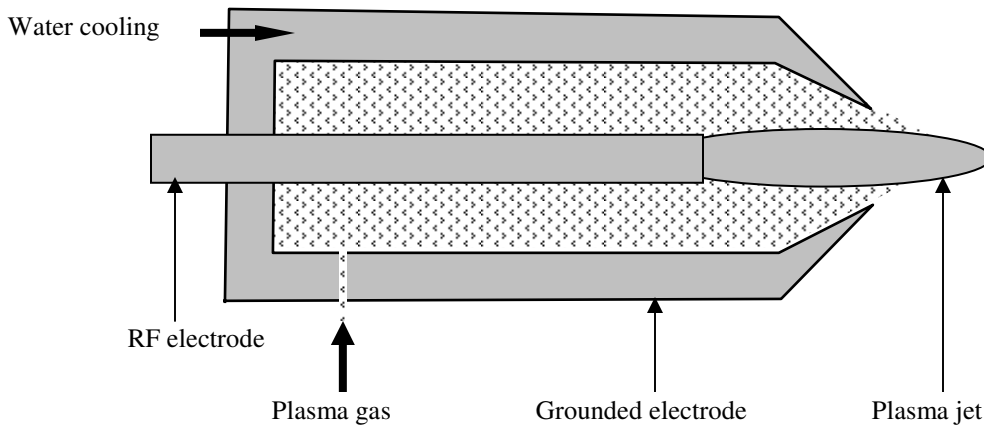


Figure 4: Schematic of atmospheric pressure plasma jet

3.3 Microhollow cathode discharge

A third approach to generate ANTP relies on the use of micro-hollow cathode electrode concept. The general idea is that the modification of cathode shapes in linear discharge lead to an increase in the current density by several orders of magnitude as compared to linear discharge. This kind of discharge with modified cathode is known as hollow cathode discharge (HCD). HCD [33] consists of a cathode, which contains some kind of a hole or a cavity or it may be a hollow cylinder, spherical segment or simply a pair of plane parallel plates, and an arbitrary shaped anode. The hollow cathode effect was originally used as a high current density electron source at low gas pressure for the development of high power pseudospark switches. The chief causes of electron generation in hollow cathodes include: (1) secondary electron emission from cathode due to ions and ultraviolet photons; (2) secondary electron emission due to bombardment of metastable atoms on the cathode, however, their flux flowing to the cathode is much smaller than that of ions; (3) pendulum or pendel effect for oscillatory motion of electrons between the opposite cathode surfaces under the influence of positive plasmas. In a specific range of values for the product pD , where p is the pressure and D the diameter of cathode bore, the current is enhanced by the pendulum motion of electrons. From a fundamental perspective, high-pressure operation of HCD can be accomplished by reducing the diameter of the bore to the values of the order of a few tens of micrometers; this hollow cathode effect can be obtained at atmospheric pressure. Thus, for atmospheric pressure discharges in hollow cathode, the typical hole diameter should be in micrometer range and

hence the term microhollow cathode discharge [34-38] arises because of the required small size of the cathode opening for high-pressure operation.

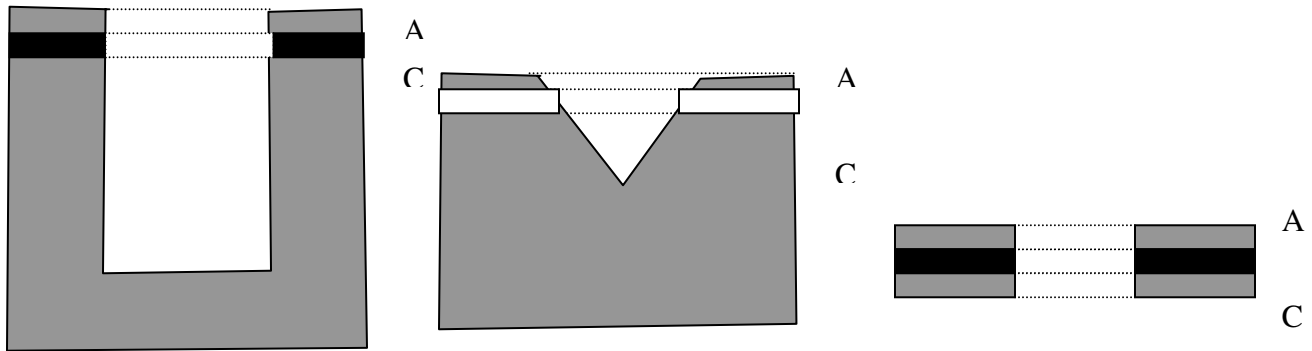


Figure 5: Typical electrode geometries of micro hollow cathode discharge [38]

The MHCD plasma may be operated in either direct current or pulse mode and two scaling laws largely determine its properties. The product (pd) of the pressure, p , and anode-cathode separation d obeys the well-known Paschen law, which determines the required breakdown voltage for a given value of p and d as well as the identity of the operating gas. A second scaling law, unique to the HCD involves the product (pD) in which D is the dimension of an aperture to the cathode. The similarity law for HCD is the basic effort to extend the pressure range for the hollow cathode discharge operation. The typical electrode geometries of MHCD are shown in fig.5. In fact, MHCDs are direct current high pressure, gas discharges between two plane parallel electrodes separated by thin layers of a dielectric material with a central borehole in each electrode. The thickness of the electrode material and the dielectric layers is in the range of $100\mu\text{m}$, while the hole diameter varies between $100\text{-}200\mu\text{m}$. MHCD plasmas have been utilized for several applications including remediation of gaseous pollutants, medical sterilization and biological decontamination, cleaning of metallic surfaces, diamond deposition etc. In addition to these applications, energetic electrons created by pendel effect efficiently generate excimers in MHCD. Such excimer sources can be operated over a wide range of wavelength in the ultraviolet and vacuum ultraviolet region.

3.4 Dielectric barrier discharge

Dielectric barrier discharge, also referred to as barrier discharge or silent discharge is a specific type of AC discharge, which provides a strong thermodynamic, non-equilibrium plasma at atmospheric pressure, and at moderate gas temperature. It is produced in an arrangement consisting of two electrodes, atleast one of which is covered with a dielectric layer placed in their current path between the metal electrodes. The presence of one or more insulating layer on/or between the two powered electrodes is one of the easiest ways to form non-equilibrium atmospheric pressure discharge. Due to the presence of capacitive coupling, time varying voltages are needed to drive the DBD. One of the major difference between the classical and a DBD discharge is that in a classical discharge, the electrodes are directly in contact with the discharge gas and plasmas, and therefore during the discharge process, electrode etching and corrosion occurs. On the contrary, in DBDs the electrode and discharge are separated by a dielectric barrier, which eliminates electrode etching and corrosion. Another fundamental difference is that the DBDs cannot be operated with DC voltage because the capacitive coupling of dielectric requires an alternating voltage to drive a displacement current. An AC voltage with amplitude of $1\text{-}100\text{ kV}$ and a frequency from line frequency to several megahertz is applied to DBD configurations. DBD cold plasma can be produced in various working mediums through ionization by high frequency and high voltage electric discharge. The DBDs unique combination of non-equilibrium and quasi-continuous behavior has motivated a wide range of applications and fundamental studies.

3.4.1 DBD Structure

The discharge burning [39-43] between two electrodes, at least one electrode insulated with a dielectric layer can be operated in a wide range of geometrical configurations such as the classical volume discharge, surface discharge, and coplanar discharge.

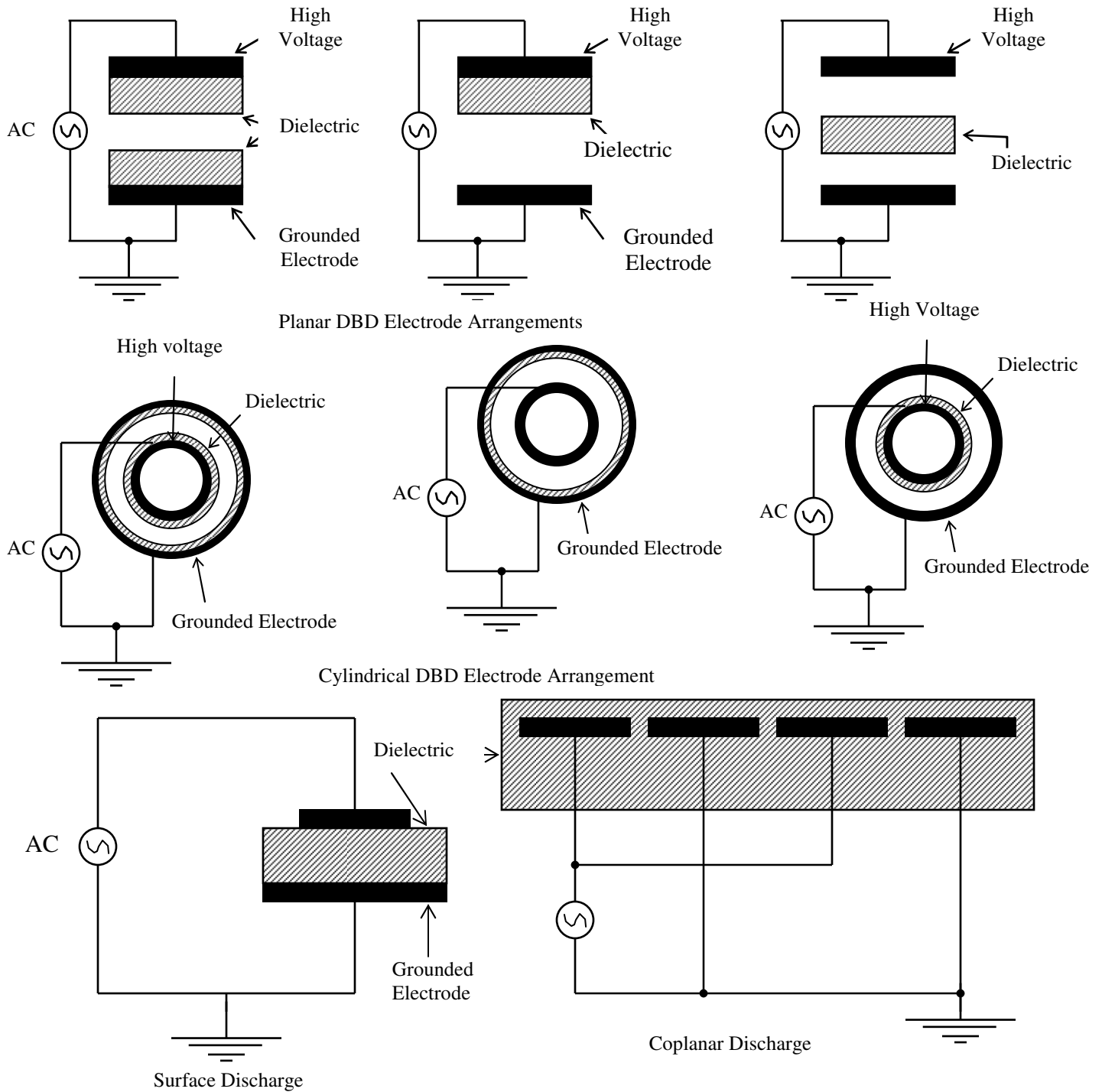


Figure 6: Typical electrode arrangements of DBD configurations

Volume discharges can also have either planar or coaxial arrangements. In planar electrode arrangements, the two electrodes are parallel to each other, and one or two dielectric barriers are always located either (i) on the powered or the ground electrode, or (ii) on both the electrodes, or (iii) in between the two metal electrodes. The electrodes in DBD can also be arranged in a coaxial manner having one electrode inside the other with at least one or two dielectric barriers located either (i) on the outer side of the inner electrode/on the inner side of the outer electrode, or (ii) on both the electrodes facing each other, or (iii) in between the two cylindrical electrodes. Besides the volume discharges, other designs also exist that use either surface or coplanar discharge geometry. Surface discharge [44] device have a thin and long electrode on a dielectric surface and an extended counter-electrode on the reverse side of the dielectric. In this configuration, the discharge gap is not clearly defined and so the discharge propagates along the dielectric surface. There also exist combinations of both volume and surface discharge configuration such as the coplanar arrangement [45-46] used in plasma display panel. The coplanar discharge device is characterized by pairs of long parallel electrodes with opposite polarity, which are embedded within a dielectric bulk nearby a surface. In addition to these configurations, other variants of DBD [47] are also used in various applications. The typical arrangements of DBD are shown in fig. 6. DBD can exhibit two major discharge modes [48-49], either filamentary mode, which is the common form of discharge composed of many microdischarges that are randomly distributed over the electrode surface; or homogenous glow discharge mode, also known as atmospheric pressure glow discharge mode due to similarity with dc glow discharges.

3.4.2 Applications of DBD

DBD technologies have an incredible potential [50-55] and are widely used in a large number of technical applications. The advantage of DBD over other discharges lies in having the option to work with non-thermal plasma at atmospheric pressure and a comparatively straightforward scale-up to large dimensions. Initially, this technology was utilized for ozone production for the treatment of drinking water. Since then the number of industrial applications of this type of discharge have shown a tremendous growth. Besides ozone synthesis, today the phenomenon of DBD in gases is widely used in the generation of excimer radiation in the UV/VUV spectral regions, surface treatment, in the field of environment protection, for pumping CO₂ lasers, pollution control, various thin film deposition processes, in the textile industry, and more recently in plasma display panel and in several other technological processes in science and industry.

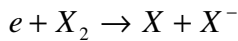
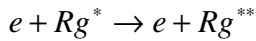
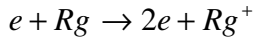
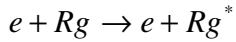
Out of all these applications of DBD, the excimer formation, one of the significant application area of DBD technology gained major impetus in the last decade. Excimer UVR optical source [56-64] is a particular configuration of DBD, specifically; a volume discharge. The acronym excimer refers to complexes with weakly bound excited state of molecules that under normal conditions do not possess a stable ground state. These excimers when they come to their ground state convert their binding energy into VUV/UV radiation. In the forthcoming section, the application of barrier discharge in this area has been elaborated.

For efficient excimer formation in non-thermal plasma (DBD & MHCD), three conditions need to be satisfied: (1) the bulk gas has to be provided with a large concentration of energetic electrons with energies above the threshold for the metastable formation or ionization; (2) since the formation of excimers is a three-body process, the gas pressure needs to be high, close to atmospheric in order to have sufficiently high rate of three body collisions. The high pressure is needed to ensure that the excimer formation reaction is faster than any quenching processes of the excited precursors; (3) the gas temperature has to be cold since excimers are thermally unstable. These conditions can only be effectively achieved in electron driven high-pressure non-thermal plasma processes occurring in DBD plasma.

The mechanism of excimer formation takes place with ionization and excitation of rare gas species by high-energy electrons. The dominant plasma chemical reactions for excimer formation can be described as follows:

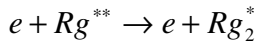
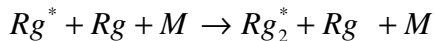
A. Electron impact ionization and excitation

The high-energy electrons in DBD ionize and excite the rare gas species. In case of rare gas halides, the high energy electrons ionize and excite the rare gas atom, and at the same time, the halogen molecules are split by a dissociative attachment reaction

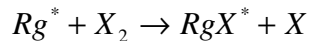


B. Formation of excimers and exciplexs

The excimer molecule is formed by three body reactions of an electronically excited rare gas atom Rg^* with other rare gas atoms or with a buffer gas in the ground state.

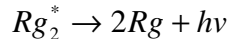


In case of rare gas/halogen mixtures, most RgX^* exciplexes are formed either by a three body ionic recombination of the positive rare gas ions and the negative halogen ions or by the Harpooning reaction in which the excited rare-gas species transfers its loosely bound electron to the halogen molecule or halogen containing compound to form an electronically excited state of RgX^* .



C. Emission of UV/VUV photon

These excimer or exciplex molecules are not very stable and once formed decompose within a few nanoseconds giving up their excitation energy in the form of UV or VUV photons.



Depending on the optical working media, a large number of different excimers can be generated in ANTP such as in DBD and MHCD.

4. CONCLUSION

In the present paper, a review of commonly used atmospheric non-thermal plasma sources has been presented. The unique features of non-thermal plasma have made possible substantial breakthroughs in many growth areas of modern technology and newer applications are continuously emerging, more recently in the vastly growing areas of nanotechnology, which indicate that the non thermal plasma has become an important player in several up-coming technologies. On the other hand, the prospect of using plasmas in numerous industrial applications without the need of any vacuum equipment has been driving the search for methods to generate atmospheric pressure non-thermal plasmas. While there is still more to go in the development and utilization of these plasma sources, no doubt that low temperature atmospheric pressure gas discharge plasma is a promising technology, not only for the future, but also for today's processes and applications. Looking ahead, still many opportunities remain to be harnessed for further research and development in order to meet the demand of various diverse plasma technological applications.

Note: T_e = electron temperature, T_i = ion temperature, T_n = neutral temperature, T_p = plasma temperature, n_e = electron density, Rg represents the ground state of rare gas species (eg., Ar, Kr, Xe, etc), X is a halogen species (eg., F, Cl, Br), Rg^* is a metastable state of neutral gas atom,

Rg_2^* is the excimer, M is a collisional third partner, which in many cases can be an atom or molecule of the active species or even of the buffer gas. The symbols, A, B stand for atoms, A_2 , B_2 for molecules, and e stands for an electron, M is a temporary collision partner, and species marked by + or – are ions, R, for a simple radical, and P, for a polymer formed in the plasma. The excited species are marked by asterisk (*), S-A indicates an atom adsorbed on the surface. The subscripts g and s indicate, respectively a species in the gas or solid phase. The term $h\nu$ indicates release of radiation energy.

5. REFERENCES

1. J. R. Roth. *Industrial Plasma Engineering: vol. 1–Principles*, IOP, Bristol and Philadelphia, (1995)
2. J. R. Roth. *Industrial plasma engineering: vol. 2, Application to non thermal plasma processing*, IOP, Bristol and Philadelphia, (2001)
3. R. Hippler, S. Pafu and M. Schmidt. *Low temperature plasma physics: Fundamental aspect and applications*, WILEY- VCH Verlag Berlin GmbH, Berlin, (2001)
4. E. E. Kunhardt. *Generation of large volume, atmospheric pressure, non equilibrium plasmas*. IEEE Trans Plasma Sci, 28: 189-199, 2000
5. A. P. Napartovich. *Overview of atmospheric pressure discharges producing non thermal plasma*. Plasmas & Polymers, 6: 1-14, 2001
6. K. H. Becker, U. Kogelschatz, R. J. Barker and K. H. Schoenbach. *Non equilibrium air plasma at atmospheric pressure*, IOP Publishing, (2004).
7. A. A. Fridman and L. A. Kennedy. *Plasma physics and engineering*, Taylor and Francis, (2004).
8. V. B. Herman. *Plasma Science and technology*, Cornell University press Ltd., London, (1982).
9. H. Conards and M. Schmidt. *Plasma generation and plasma sources*. Plasma Sources Sci. Technol., 9: 441-454, 2000
10. P. I. John. *Plasma science and creation of wealth*. Tata McGraw Hill, India 2005.
11. A. Bogaerts, E. Neyts, R. Gijbels and J. V. Mullen. *Gas discharge plasma and their applications*. Spectrochimica Acta Part B, 57: 609-658, 2002
12. M. I. Boulos, P. Fauchais and E. Pfender. *Thermal plasma: Fundamental and applications*, vol. 1, Plenum Press, New York, (1994).
13. E. Pfender. *Thermal plasma processing in nineties*. Pure Appl. Chem., 60: 591-606, 1988
14. M. I. Boulos. *Thermal plasma processing*. IEEE Trans. Plasma Sci., 19: 1078-1089, 1991
15. M. I. Boulos. *New frontiers in thermal plasma processing*. Pure Appl. Chem., 68:1007-1010, 1996

16. P. Fauchais and A. Vardelle. "Thermal plasmas". IEEE Tran Plasma Sci, 25: 1258-1270, 1997
17. E. Pfender. "Thermal plasma technology: Where do we stand and where are we going". Plasma Chem. Plasma Proc., 19: 1-31, 1999
18. N. Venkatramani. "Industrial plasma torches and applications". Current Science, 83: 254-262, 2002
19. J. Heberlein. "New approaches in thermal plasma technology". Pure Appl. Chem. 74: 327-335, 2002
20. G. Bonnizzoni and E. Vassallo. "Plasma physics and technology; industrial applications". Vacuum, 64:327-336, 2002.
21. B. Gupta, "Plasma processing: Some basic considerations. In: Plasma Physics", Wiley Eastern Limited, 170-211, 1992.
22. N St J Braithwaite. "Introduction to gas discharges". Plasma Sources Sci. Technol., 9:517-527, 2000
23. S. N. Sen. "Plasma Physics". Pragati Prakashan, India, 8-12, (2006).
24. A. Fridman, A. Chirokov and A. Gutsol. "Non-thermal atmospheric pressure discharges". J. Phys D: Appl Phys, 38: R1-R24, 2005.
25. J. S. Chang, P. A. Lawless and T. Yamamoto. "Corona discharge processes". IEEE Trans. Plasma Sci., 19:1152-1166, 1991.
26. U. Kogelschatz. "Atmospheric-pressure plasma technology". Plasma Phys. Control. Fusion, 46: B63-B75, 2004
27. A. Schutze, J. Y. Jeong, S. E. Babayan, J. Park, G. S. Selwyn and R.F. Hicks. "The atmospheric-pressure plasma jet: A review and comparison to other plasma sources". IEEE Trans Plasma Sci., 26:1685-1694, 1998.
28. J. Y. Jeong, S. E. Babayan, V. J. Tu, J. Park, I. Henins, R. F. Hicks and G. S. Selwyn.. "Etching materials with an atmospheric pressure plasmas jet". Plasma Sources Sci Technol, 7: 282-285, 1998
29. H. W. Herrmann, I. Henins, J. Park and G. S. Selwyn. "Decontamination of chemical and biological warfare (CBW) agents using an atmospheric pressure plasma jet (APPJ)". Physics of Plasmas, 6: 2284-2289, 1999
30. J. Park, I. Henins, H. W. Hermann, G. S. Selwyn. "Gas breakdown in atmospheric radio-frequency capacitive plasma source". J. Appl. Phy., 89:15-19, 2001
31. G. S. Selwyn, H. W. Herrmann, J. Park and I. Henins. "Material processing using an atmospheric pressure RF-generated plasma source". Contrib Plasma Phys., 6:610-619, 2001
32. S. E. Babayan, J. Y. Jeong, A. Schutze, V. J. Tu, M. Moravej and G. S. Selwyn "Deposition of silicon dioxide films with a non-equilibrium atmospheric pressure plasma jet". Plasma Sources Sci Technol, 10:573-578, 2001

33. A. D. White. "*New hollow cathode glow discharge*". J. Appl. Phys., 30:711-719, 1959
34. K. H. Schoenbach, A. E. Habachi, W. Shi and M. Ciocca. "*High- pressure micro hollow cathode discharges*". Plasma Sources Sci Technol, 6: 468-477, 1997
35. J. W. Frame, D. J. Wheeler, T. A. DeTemple and J. G. Eden. "*Micro discharge fabricated in silicon*". Appl. Phys. Lett., 71:1165-1167, 1997
36. K. H. Schoenbach and R. H. Stark. "*Direct current high-pressure glow discharges*". Appl Phys Lett, 72:13-15, 1998.
37. V. Nehra, C. L. Mittal and H. K. Dwivedi. "*Micro hollow Cathode Plasma Applications: From Excimer Source to Flat TV Screens*". ICFAI Journal of Science & Technology, 1: 50-62, 2005.
38. K. H. Becker, K. H. Schoenbach and J. G. Eden. "*Microplasmas and applications*". J. Phys. D: Appl. Phys., 39: R55-R70, 2006
39. B. Eliasson and U. Kogelschatz. "*Non-equilibrium volume plasma chemical processing*". IEEE Trans. Plasma Sci., 19:1063-1077, 1991
40. G. J. Pietsch. "*Peculiarities of dielectric barrier discharges*". Contrib. Plasma Phys., 41:620-628, 2001
41. U. Kogelschatz. "*Industrial innovation based on fundamental physics*". Plasma Sources Sci. Technol, 11: A1-A6, 2002
42. U. Kogelschatz. "*Dielectric-barrier discharges: Their history, discharge physics, and industrial applications*". Plasma Chem. Plasma Proc., 23:1-46, 2003
43. A. Chirokov, A. Gutsol and A. Fridman. "*Atmospheric pressure plasma of dielectric barrier discharges*". Pure Appl Chem, 77: 487-495, 2005
44. G. J. Pietsch and C. Humpert. "*Discharge mechanism and ozone generation by surface discharges depending on polarity.*" In HAKONE 8th International Symposium on High Pressure Low Temperature Plasma Chemistry, Puhajarve Estonia, 2002.
45. L. Hulka and G. J. Pietsch. "*On the ignition voltage and structure of coplanar barrier discharges*". In HAKONE 8th International Symposium on High Pressure Low Temperature Plasma Chemistry, Puhajarve Estonia, 2002.
46. V. I. Gibalov, T. Murata and G. J. Pietsch. "*Parameters of barrier discharges in coplanar arrangements*". In HAKONE 8th International Symposium on High Pressure Low Temperature Plasma Chemistry, Puhajarve Estonia, 2002.
47. Y. H. Lee and G. Y. Yeom. "*Properties and applications of a modified dielectric barrier discharge generated at atmospheric pressure*". Jpn. J. Appl. Phys., 44: 1076-1080, 2005.
48. U. Kogelschatz. "*Filamentary, patterned and diffuse barrier discharges*". IEEE Trans. Plasma Sci., 30:1401-1407, 2002.
49. T. Nozaki, Y. Unno, Y. Miyazaki and K.Okazaki. "*A clear distinction of plasma structure between APG and DBD, paper*" presented to 15th International Symposium on Plasma Chemistry, Orleans, France, 2001.

50. X. Xu. "*Dielectric barrier discharge-properties and applications*". Thin Solid Films, 390: 237-242, 2001.
51. U. Kogelschatz, B. Eliasson and E. Walter. "*From ozone generator to flat television screens: history and future potential of dielectric barrier discharges*". Pure Appl. Chem., 71:1819-1828, 1999.
52. U. Kogelschatz, M. Hirth and B. Eliasson. "*Ozone synthesis from oxygen in dielectric barrier discharges*". J. Phys. D: Appl. Phys., 20: 1421-1437, 1987.
53. U. Kogelschatz. "*Silent discharges for the generation of ultraviolet and vacuum ultraviolet excimer radiation*". Pure Appl. Chem, 62:1667-1674, 1990.
54. El Dakrouri, J. Yan, M. C. Gupta, M. Laroussi and Y. Badr "*VUV emission from a novel DBD based radiation source*". J Phys D Appl Phys, 35:L109-L114, 2002.
55. H. E. Wagner, R. Brandenburg, K. V. Kozlov, A. Sonnenfeld, P. Michel, J. F. Behnke. "*The barrier discharge: basic properties and application to surface treatment*". Vacuum, 71: 417-436, 2003.
56. I. W. Boyd, Z. Y. Zhang U. Kogelschatz. "*Development and applications of UV excimer lamps, Photo-Excited Processes, Diagnostics and Applications.*", A. Peled, Ed., 161-199, Kluwer Academic, The Netherlands, (2003).
57. U. Kogelschatz. "*Excimer lamp: Their history, discharge physics and industrial applications*". In Proceedings of the SPIE, 5483:272-286, 2004.
58. M. I. Lomaev, E. A. Sosnin, V. F. Tarasenko, D. V. Shitts V.S. Skakun and M. V. Erofeev. "*Capacitive and barrier discharge excilamps and their applications*". Instruments & experimental technique, 49:595-746, 2006.
59. V. F. Tarasenko. "*Excilamps as efficient UV-VUV light sources*". Pure Appl. Chem., 74: 465-469, 2002.
60. M. I. Lomaev, V. S. Skakun, E. A. Sosnin, V. F. Tarasenko, D. V. Shitts and M. V. Erofeev. "*Excilamps: efficient sources of spontaneous UV and VUV radiation*". Instruments and methods of investigation, 28:1-17, 2002.
61. T Oppenlander, "*Potentials and Applications of Excimer Lamps (Incoherent Vacuum-UV/VUV Sources) in Photochemistry and in Photochemical Technology*" <http://www.stp-gateway.de/start/start2.html>
62. J. Y. Zhang, I. W. Boyd. "*Lifetime investigation of excimer UV source*". Appl. Surf. Sci., 168:296-299, 2000.
63. Y. Morimoto, T. Sumitomo, M. Yoshioka, T. Takemura. "*Recent progress on UV lamps for industries*". Industry Application Conference, IAS, IEEE, 2: 1008 -1015, 2004
64. T. Oppenlander and E. Sosnin. "*Mercury free (VUV) and UV excil lamps: lamps of the future*". IUVA news, 7: 16-20, 2005.

COMPUTER SCIENCE JOURNALS SDN BHD
M-3-19, PLAZA DAMAS
SRI HARTAMAS
50480, KUALA LUMPUR
MALAYSIA